Microstructure, Micro-inclusions and Mineralogy along the EGRIP ice core - Part 1: Localisation of inclusions and deformation patterns

Nicolas Stoll[1], Jan Eichler[1], Maria Hörhold[1], Tobias Erhardt[1, 2], Camilla Jensen[2], and Ilka Weikusat[1, 3]

[1]Alfred Wegener Institute Helmholtz Centre for Polar and Marine Research, Bremerhaven, Germany
[2]Climate and Environmental Physics, Physics Institute and Oeschger Centre for Climate Change Research, University of Bern, Bern, Switzerland
[3]Department of Geosciences, Eberhard Karls University, Tübingen, Germany

Correspondence: Nicolas Stoll (nicolas.stoll@awi.de)

Abstract. Impurities deposited in polar ice allow the reconstruction of the atmospheric aerosol concentration of the past. At the same time they impact the physical properties of the ice itself such as its deformation behaviour. Impurities are thought to enhance ice deformation, but observations are ambiguous due to a shortage of comprehensive microstructural analyses. For the first time, we systematically analyse micro-inclusions in polar fast flowing ice, i.e. from the East Greenland Ice Core Project ice core drilled trough the Northeast Greenland Ice Stream. In direct relation to the inclusions we derive the crystal-preferred orientation, fabric, grain size, and microstructural features at ten depths, covering the Holocene and Late Glacial. We use optical microscopy to create microstructure maps to analyse the in situ locations of inclusions in the polycrystalline, solid ice samples. Micro-inclusions are more variable in spatial distribution than previously observed, and show various distributional patterns ranging from centimetre-thick layers to clusters and solitary particles, independent of depth. Analysing the area occupied by grain boundaries in the respective samplesshows that micro-inclusions are slightly In half of all samples, micro-inclusions are more often located at or close to grain boundaries in half of all samplesthe grain boundaries by a slight margin (in the areas occupied by grain boundaries). Throughout all samples we find strong indications of dynamic recrystallisation, such as grain islands, bulging grains and different types of subgrain boundaries. We discuss the spatial variability of micro-inclusions, the link between spatial variability and mineralogy, and possible effects on the microstructure and deformation behaviour of the ice. Our results emphasise the need for holistic approaches in future studies, combining microstructure and impurity analysis.

1 Introduction

Polar ice sheets are key elements of our climate system and deep ice cores from these regions are used, but not limited, to reconstruct the paleoclimate (e.g., Dahl-Jensen et al., 2013; EPICA Community Members, 2004) (e.g., Lorius et al., 1985; Petit et al., 1999; Watanabe et al., 2003; EPICA Community Members, 2004; Dahl-Jensen et al., 2013) and to investigate the dynamics of ice in ice sheets (e.g., Alley, 1988; Weikusat et al., 2017a). The atmospheric aerosol concentration is partly imprinted in the

snow at the surface. As the snow transforms to ice, the deposited aerosols either dissolve in the ice structure or form micro-inclusions. With time they get transported into deeper regions in the ice sheet. As ice crystals are separated by dynamically changing interfaces, i.e. grain boundaries, they undergo constant changes in response to stress and strain resulting in different

25 crystal shapes, sizes, and orientations. Therefore ice cores enable the gathering of information about the internal deformation of polar ice and its mechanisms, as the localised characteristics determine the large-scale deformation behaviour.

The deformation characteristics of ice strongly impact the flow of ice sheets. The quality of future projections of the ice sheets and their ice flow under changing climate conditions strongly ~~depend~~ depends on the understanding of ice dynamics on all scales. Especially the mechanisms controlling fast flowing ice stream dynamics and the relation to the slow-moving ice

30 outside the ice streams is insufficient (Minchew et al., 2018, 2019; Stearns and van der Veen, 2019).

To improve the understanding of large-scale ice dynamics processes in the microstructure of ice, i.e. on the millimetre- and centimetre-scale, have to be understood as they control the strain rate. The main deformation process of ice crystals is dislocation creep, which describes the movement of dislocations in the basal plane in combination with climb (Glen and Jones, 1967; Weertman, 1973; Hobbs, 1974; Petrenko and Whitworth, 1999). The preferred orientation of crystals plays an important

35 role for the deformation of ice, however, under certain boundary conditions, it is further impacted by other properties such as grain size (e.g., Goldsby and Kohlstedt, 1997; Cuffey et al., 2000; Kuiper et al., 2020b), crystal preferred orientation (CPO), and also impurity content (e.g., Glen and Jones, 1967; Jones and Glen, 1969; Fisher and Koerner, 1986). The relationship between CPO, grain size, and impurity content and how they impact deformation is still under debate (Stoll et al., 2021b). Nevertheless, the impact of impurities on the microstructural deformation has been shown to play a significant role and needs

40 further investigation.

In this study, we define impurities as extrinsic chemical compounds found in the ice which can be separated into soluble and insoluble impurities. They were deposited on the ice sheet and originated from a variety of atmospheric aerosols with unique transport histories (Legrand and Mayewski, 1997; Weiss et al., 2002). Soluble impurities dissolve in the lattice and originate from dissolved gases or from salts dissociated into ions (Legrand and Mayewski, 1997; Della Lunga et al., 2014). Those

45 impurities are chemical compounds and elements of diverse origin (marine, terrestrial, biological, atmospheric). Insoluble impurities consist of lattice-incoherent phases and are rejected from the ice lattice (Ashby, 1969; Alley et al., 1986a). They are often from terrestrial origin, such as dust, and vary in size, ranging from micrometre-sized "micro-inclusions" to large dust particles (Steffensen, 1997; Wegner et al., 2015; Simonsen et al., 2019).

Impurities impact the physical properties of snow, firn, and ice at all depths, ranging from permittivity (Wilhelms et al.,

50 1998) to electrical conductivity (Alley and Woods, 1996; Wolff et al., 1997), and mechanical properties (Dahl-Jensen and Gundestrup, 1987; Paterson, 1991; Weiss et al., 2002; Hörhold et al., 2012; Fujita et al., 2014; Moser et al., 2020). Especially the impact of impurities on the deformation of ice has been investigated for decades (e.g., Jones and Glen, 1969; Petit et al., 1987; Fukazawa et al., 1998; Iliescu and Baker, 2008; Eichler et al., 2019; Stoll et al., 2021b). Impurities can have indirect effects on the deformation of ice, i.e. they affect stress accommodating mechanisms such as recrystallization. In this case, the

55 microstructure (grain shape and size) is impacted by impurities, which control grain boundary mobility, energy, and length by e.g., dragging of grain boundaries (Alley et al., 1986a, 1989) or Zener pinning (Smith, 1948; Humphreys and Hatherly,

2004). Impurities can have a direct impact by multiplying dislocations or increasing their mobility. This happens when there are obstacles, such as micro-inclusions, in the ice matrix which produce strain localisation and thus new dislocation lines (Weertman and Weertman, 1992), or occupy lattice sites introducing protonic defects (Glen, 1968).

60 Thus, understanding the microstructural impurity localisation is significant regarding dielectric properties (Stillman et al., 2013), the stratigraphic integrity of impurity records in deep polar ice (Faria et al., 2014a; Ng, 2021), and deformational properties (e.g., Dahl-Jensen et al., 1997; Barnes et al., 2002a; Della Lunga et al., 2014; Eichler et al., 2017; Shigeyama et al., 2019). Ice core impurity content in ice cores is often measured by meltwater analysis such as continuous melt water analysis (CFA) (e.g., Röthlisberger et al., 2000; McConnell et al., 2002; Kaufmann et al., 2008), and/or Ion Chromatography (e.g.,

65 Cole-Dai et al., 2006; Severi et al., 2014). However the information on the in situ microstructural localisation, composition, and form of impurities is lost.

Samples from several ice cores have been analysed with methods enabling the location of impurites, such as optical microscopy (e.g., Kipfstuhl et al., 2006; Faria et al., 2010; Eichler et al., 2017), Scanning Electron Microscope (SEM) coupled with energy dispersive X-ray spectroscopy (EDS) (e.g., Cullen and Baker, 2000; Barnes et al., 2002a; Obbard and Baker,

70 2007), LA-ICP-MS (e.g., Reinhardt et al., 2001; Della Lunga et al., 2014; Spaulding et al., 2017; Bohleber et al., 2020) and Raman spectroscopy (e.g., Ohno et al., 2005; Sakurai et al., 2011; Ohno et al., 2014; Eichler et al., 2019). Results were diverse, and often ambiguous, and were recently summarised by Stoll et al. (2021b). A major impediment is the often small number of analysed samples and limited amounts of measured impurities. Furthermore, samples often originate from more or less arbitrary depths, allowing glimpses into specific depth regimes with highly variable boundary conditions (e.g., age, bulk impurity

75 content). Discussed generalisations of spatial distribution and the drawn conclusions on deformation effects were seldom based on systematic analyses, i.e. along a specific section of an ice core. Furthermore, the large variety in applied methods, sample origins and analysed impurity forms (soluble, insoluble, elements, compounds) impede the drawing of reliable conclusions for polar ice in general. Stoll et al. (2021b) concluded that, among others, structured methodological approaches are needed to enhance our understanding of the role of impurities regarding the deformation of ice. One promising approach is a systematic

80 high-resolution analysis of one deep ice core combining methods from microstructure and impurity research.

Even though impurities do play a significant role in ice deformation, the specific species or processes are not understood, also due to limitations by measurement techniques or previous measurement set-ups. Which minerals are found throughout polar ice? In which state are impurities found and does their state influence their location in respect to grain boundaries and the crystal lattice? And finally, which of these (and probably many others) properties impact the deformation rate of ice and are

85 they vice-versa affected by deforming ice? The on-going East Greenland Ice Core Project (EGRIP) located on the Northeast Greenland Ice Stream (NEGIS) is a chance to address these ~~question~~ questions. The EGRIP core is the first deep ice core from an ice stream and thus an unique possibility to study ice dynamics in detail as displayed in recent CPO and visual stratigraphy data (Westhoff et al., 2020).

Addressing these interdisciplinary questions is extensive work and thus presented in two companion papers. In this study

90 we investigate the localisation of visible micro-inclusions and deformation patterns along the EGRIP ice core while ~~a second study analyses~~ Stoll et al. (2021a) analyse the mineralogy of these micro-inclusions. Here we apply optical microscopy and automated
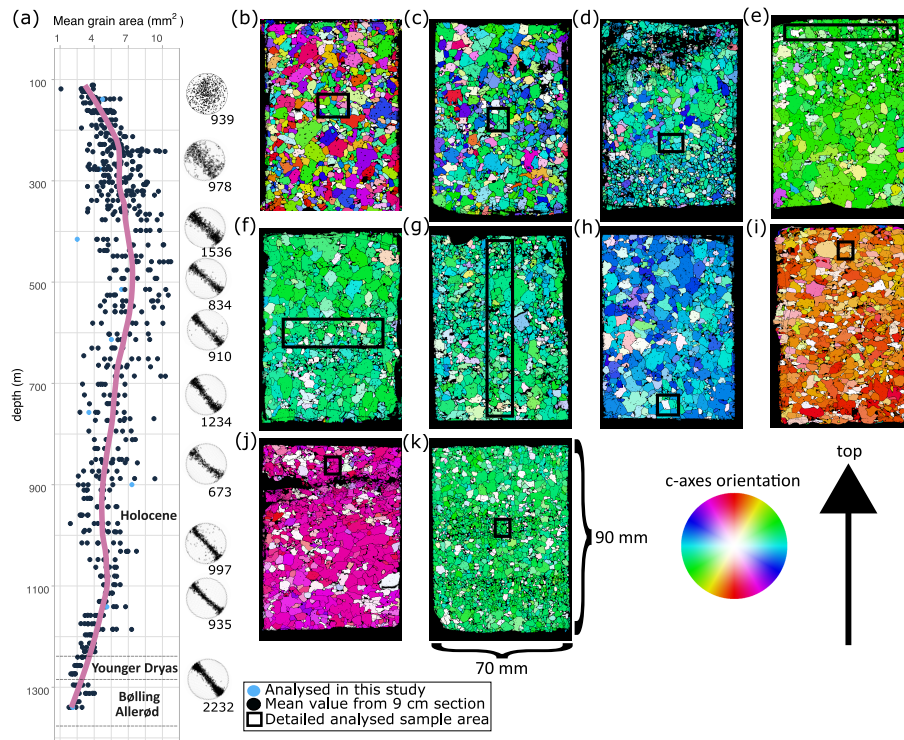
Figure 1. Grain size, CPO and fabric data from the upper 1340 m of the EGRIP ice core. a) Bag 9 cm section mean grain sizes derived via FA G50. The violet line is a locally weighted regression with a smoothing parameter of 0.3. C-axis orientations of each section projected into a horizontal plane rotated towards their most likely position (Westhoff et al., 2020), the true orientation was lost during drilling. The number is c-axes per section. b)-k) Fabric data from the analysed thin sections. The colour code (legend) indicates the c-axes orientation, vertical c-axes appear white. Fabric image surfaces are not the same as in impurity maps due to sample processing and the focusing into the sample. Black areas are background corrections.

fabric analyser measurements with related statistical analysis of the microstructure on ten samples covering Holocene and Late Glacial ice. We aim to give a systematic overview of the microstructural locations of micro-inclusions and of the evolution of the microstructure and discuss mineralogy-depended spatial patterns. Finally, we elaborate the effects of micro-inclusions on the deformation behaviour as seen in the microstructure of the EGRIP ice core.

2 Methods

2.1 The East Greenland Ice Core Project

EGRIP is an ice core drilling project located on NEGIS, the largest ice stream in Greenland which terminates in three outlet glaciers (Nioghalvfjerds isstrommen, Zachariae isbrae and Storsstrommen) (Joughin et al., 2010; Vallelonga et al., 2014). The
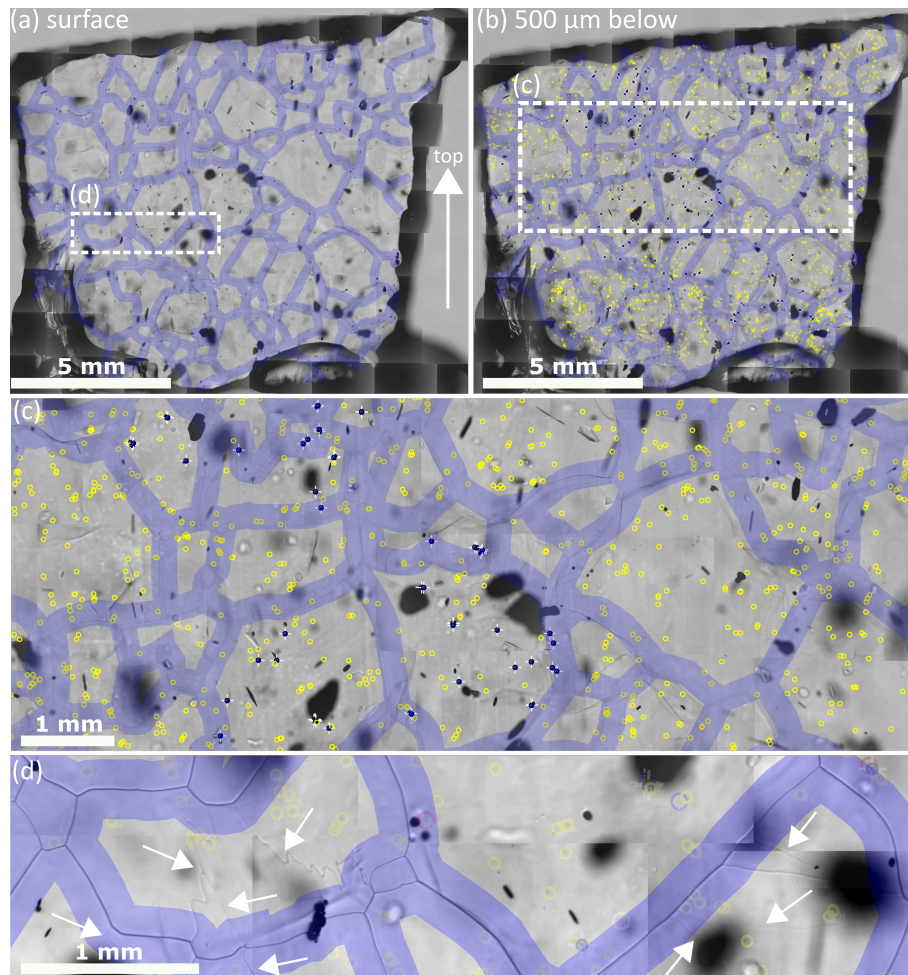
Figure 2. Details of the analysis procedure on the sample from a depth of 1339.75 m. Grain boundaries are indicated with 300 μm thick violet lines. Localised micro-inclusions 500 μm below the surface are indicated by yellow circles. Micro-inclusions analysed with Raman spectroscopy in a companion paper by Stoll et al. (2021a) are indicated by blue circles with white crosses. Out of focus black shapes are air bubbles. A) Map of the sample surface with highlighted grain boundaries, the arrow indicates the surface of the ice sheet. B) Impurity map with a focus depth of 500 μm below the sample surface, micro-inclusions and grain boundaries are indicated. C) Detail of the area indicated in B. D) Detail of the area indicated in A with different types of subgrain boundaries indicated by white arrows. Subgrain boundaries are more common in larger grains and rarely close to micro-inclusions.

drill camp was located at 75°38' N and 35°58' W in 2015, 2704 m a.s.l., 440 km to the South-East of the North Greenland Eemian Ice Drilling (NEEM) site. Ice flow velocity at the drill site is 55 m a^{-1} (Hvidberg et al., 2020). Drilling has started in 2016 and has been continued in the summer seasons of 2017, 2018, and 2019. The 2019 drilling season stopped at a depth of 2121 m, approximately 530 m above bedrock. At EGRIP the brittle ice zone is between 550 and 1000 m of depth according to Visual Stratigraphy and the core break record. Following Walker et al. (2018) the Holocene (present-11.7 ka) is in the upper

105 1240 m, the Younger Dryas (11.7-12.8 ka) at 1240-1280 m, and the Bølling Allerød (12.8-14.7 ka) at 1280-1375 m (Mojtabavi et al., 2020). We focus on the analysis of the upper 1340 m in this study.

2.2 Physical properties measurements

At EGRIP every 5-15 m fabric and microstructure measurements were performed continuously on 55 cm long sections ("bags"). Thick and thin sections (~90 mm length x 70 mm width x 0.3 mm thickness) were prepared and measured in situ in the EGRIP
110 trench (-18°C). Thin sections were measured in 20 μm resolution with an automated fabric analyser (Wilson et al., 2003) (FA G50) from Russell-Head Instrument and grain size and CPO data (Fig. 1A) was were obtained by digital image processing (Eichler, 2013). Grain sizes in each thin section were derived by the automated detection of grain boundaries and grains. The measured grain cross-sectional area is the number of pixels forming one grain (minimum grain size: 500 pixels) as described by Eichler (2013). The average grain size per section was used to determine the arithmetic mean grain size of each bag.

115 2.3 Sample choice and preparation

Samples and specific regions of interests interest for microstructural impurity analysis were defined using CFA (companion paper)(Stoll et al., 2021a), grain size and crystal orientation data (Fig. 1) . If possible, samples simultaneously included different with the aim to give an overview of the Holocene. Samples with high dust particle concentrations while simultaneously including different microstructural and fabric properties (e.g., small and large grains)and different c-axes orientations) were chosen. We analysed
120 ten samples in detail between depths of 138.92 and 1339.75 m (Fig. 1 and Table 2). The nine shallower samples are from the Holocene and the deepest sample is from the last glacial termination, i.e. the Bølling Allerød (Mojtabavi et al., 2020).

We used the remaining ice of the physical properties samples analysed at the EGRIP camp and followed the standard procedure by Kipfstuhl et al. (2006) to create thick sections with a thickness of ~10 mm. Contrary to Kipfstuhl et al. (2006) we did not use silicon oil, which produces intensive Raman spectra and can mask the micro-inclusion spectra. Different sample
125 sizes were used, but most samples were approximately 10 x 10 mm (Table 2) and the surface and bottom of the samples were polished with a Leica microtome. Each polishing was followed by 1.5-2 hours of sublimation under controlled temperature and humidity conditions to obtain a good sample surface quality. Thus, grain-boundary grooves became more distinct and were easier to detect while small-scale disturbances (e.g., microtome scratches) were erased. Flawless surfaces enable the localisation of micro-inclusions inside the sample (500 μm below the surface) to produce high-quality microstructure maps.

130 2.4 Microstructure mapping and impurity maps

Microstructure mapping was performed following Kipfstuhl et al. (2006) and Eichler et al. (2017). Samples were placed under an optical Leica DMLM microscope with an attached CCD camera (Hamamatsu C5405), a software-controlled x-y stage and a frame grabber. The scanning resolution was 3 μmpix^{-1} and several hundred individual photomicrographs were created gridwise. This enabled the creation of high-resolution maps to detect micro-inclusions. These maps also provide the basis for a
135 companion structured Raman spectroscopy study proving that the mapped dots are chemical impurities, i.e. micro-inclusions (Stoll

et al., 2021a). Micro-inclusions are dust particles, droplets and salts inside the ice matrix and probably the most common form of impurity incorporations in ice. They are of the size of typical dust particles (1-2 μm) (Wegner et al., 2015) and are close to the resolution limit of the microscope. Transmission light mode and different focus depths enabled us to focus inside the ice and to locate micro-inclusions below the surface (Fig. 2). The optical resolution of the photographs hampers the identification

140 of the shape or volume of micro-inclusions. Locations of micro-inclusions were mapped manually following Eichler et al. (2017) which provides an "impurity map". Other features in the ice were visually identified as plate-like inclusions (caused by relaxation) (Nedelcu et al., 2009) and gas inclusions (air bubbles and clathrate hydrates) (Ohno et al., 2010; Weikusat et al., 2012) (Fig. 5C).

Impurity maps enable a structured and fast localisation of micro-inclusions with a confocal Raman microscope, which
145 otherwise would be tedious in impurity-poor Holocene ice. They further allow the identification of micro-inclusions in the microstructure and thus preserve important spatial information. Grain boundaries were mapped on the sample surface and translated to the impurity map (Fig. 2). We applied a grain boundary width of 100, 200, and 300 μm and chose 300 μm as our reference for further analysis to compensate for light diffraction with depth and vertically tilted grain boundaries as done by Eichler et al. (2017). We created microstructure maps of all samples and located micro-inclusions in all of them.
150 Micro-inclusions located in the 300 μm large grain boundary area are classified as "at the in the vicinity of the grain boundary" and serve as upper-limit upper limit assumptions.

Small grains might enhance the probability of micro-inclusions being located close to grain boundaries. To compare samples with different grain sizes we measured the total area occupied by grain boundaries per sample for ten samples resulting in the ratio of micro-inclusions in the vicinity of grain boundaries to grain boundary area to micro-inclusions at grain boundaries (R_{GB}):

$$R_{GB} = \frac{I_{GB}}{A_{GB}} \tag{1}$$

I_{GB} is the percentage of micro-inclusions at in the vicinity of grain boundaries, and A_{GB} is the accumulated area occupied by grain boundaries per sample in percent using the upper limit assumption. A ratio of 1 implies a coherent relation of micro-inclusions at in the vicinity of grain boundaries, while R<1 implies less micro-inclusions at in the vicinity of grain boundaries than assumed from the grain boundary area of the sample, R>1 implies the opposite, i.e. more micro-inclusions at in the vicinity
160 of grain boundaries than implied by the grain boundary area. Furthermore, we performed a two-sided binomial test to derive the statistical significance of micro-inclusions being located at in the vicinity of grain boundaries. The amount of micro-inclusions at in the vicinity of grain boundaries and the area occupied by grain boundaries were used to calculate the respective p-value.

3 Results

3.1 Evolution of grain size, CPO and microstructure with depth

165 We derive a profile of the grain size with depth, displaying the grain size evolution of the upper 1340 m of the EGRIP ice core and microstructural data from the depth regimes analysed with optical microscopy (Fig. 1).

Grain size: The mean grain sizes derived from the EGRIP core per 55 cm bag vary between 2.21 and 10.8 mm^2 (Fig. 1A). Starting from 3.9 mm^2 at the depth of 111 m, it steadily increases in the shallowest part and peaks around 500 m. Grain size decreases uniformly until 900 m, where it remains at ~4.75 mm^2 until 1100 m of depth. The following 260 m are characterised by a steady decrease towards the minimum grain size of 2.21 mm^2.

We find the grain size to be highly variable on the centimetre-scale, mean values from neighbouring bags can vary up to 5 mm^2 (e.g., at 240 and 540 m). This occurs primarily in the shallower part of the Holocene ice, mean grain size values are more similar towards the Last Glacial (Fig. 1A). Fabric images (Fig. 1B-K) display the high variety of grain size on the centimetre-scale. Some samples show layers of very fine grains (e.g., Fig. 1F, G and K).

The grain size distribution within the ten analysed thin sections is displayed in Fig. 3. Median grain sizes vary between 1.02 (1339.75 m) and 2.04 mm^2 (139.92 m) and mean grain sizes range from 2.11 (1339.75 m) to 7.31 mm^2 (899.98 m). All samples show an uneven, skewed right distribution with a tail towards larger grain sizes; mean values are higher than medians.

Crystal preferred orientation: The analysed samples show a clear CPO evolution with depth. The shallowest sample shows a broad single maximum, which develops into a vague vertical girdle at 276 m. With depth, the girdle increases in strength and is a fully developed vertical girdle below 1141 m (Fig. 1). Numbers of c-axes per sample vary between 673 and 1536 in the upper 1141 m. The deepest sample from a depth of 1339.75 m has 2232 measured c-axes orientations as a result of the small grain size in the last Glacial Termination and a thus higher number of grains per sample.

Microstructure: Common microstructural features in the upper 1340 m of the EGRIP ice core are subgrain boundaries (border regions of slightly different misorientations), bulging grains, grain islands (new grains inside highly distorted parent grains), and irregular shaped grains. Examples of these features from all depths are shown in Fig. 4. Subgrain boundaries are distributed heterogeneously in most grains in different intensities and shapes. Shapes range from normal or parallel to the basal plane to irregular zigzag patterns. These different types of subgrain boundaries often occur in the same grain. A few strongly developed subgrain boundaries were observed to cross grains completely independently of grain shape. Large grains usually inhibit more subgrain boundaries than small grains. Most grains are sharply or smoothly curved and grains often bulge towards grains with higher amounts of subgrain boundaries. Occasionally well developed (sub-)grain islands (Fig. 4G) were observed, mainly in large grains with protruding grain boundaries.

3.2 Localisation of micro-inclusions

In total, 5728 micro-inclusions (small yellow circles in Fig. 5) were located within ten analysed samples. In total, the spatial distribution of micro-inclusions in EGRIP ice is highly variable and micro-inclusions are heterogeneously distributed (Fig. 7). They have been found, solitary or in clusters, at in the vicinity of grain boundaries, triple junctions and in the grain interior (Fig. 5). Distinct spatial distributional patterns have been observed throughout the core in varying strength and number, but no clear trend regarding preferred locations could be derived. No relationship between micro-inclusion distribution and depth was observed. However, the spatial distribution differs significantly depending on the examined scale as displayed in Fig. 5 and Fig. 7.
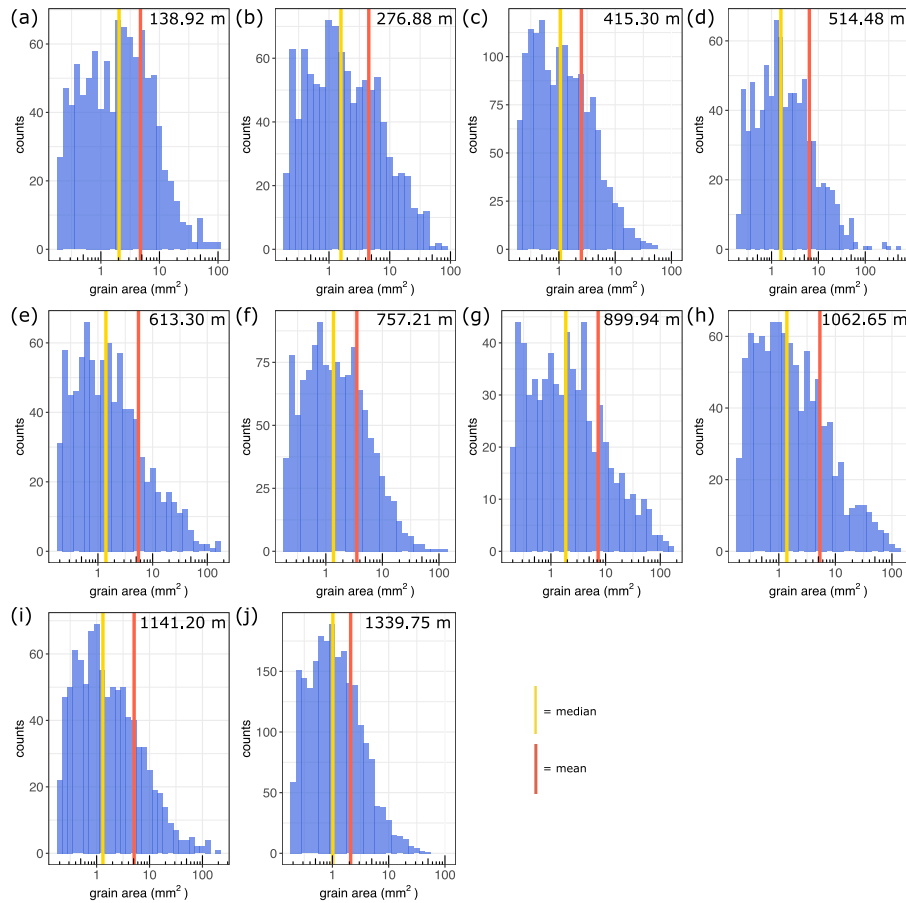
Figure 3. Grain size distribution within the 9 cm long physical properties samples. The indicated depths refer to the middle of the sample. Note the varying counts on the y-axis.

On the centimetre-scale layers of high micro-inclusion concentration were observed. However, regions with few micro-inclusions were also observed, e.g., at 415.3 m (see Table 2 column n_{mi}). On the millimetre-scale a variety of spatial distribution patterns was observed. Micro-inclusions form clusters (defined as three or more very close inclusions) and chains (Fig. 5B and C), which can extend over grain boundaries. Isolated inclusions were found in different distances to other micro-inclusions, ranging from micrometers to several millimetres (sometimes across grain boundaries). On the micrometre-scale several spatial patterns of micro-inclusions were observed. Inclusions were found in clusters of up to 4-5 single inclusions, in horizontal bands of varying lengths and at remote locations far away from other inclusions (Fig. 5B and C). Furthermore, large differences in the spatial distribution of micro-inclusions were observed from grain to grain. Grains with a high number of micro-inclusions are often neighboured by grains with only a few, or even zero, micro-inclusions despite being at the same depth. The amount of micro-inclusions does not seem to be related to the orientations of the crystals. Micro-inclusions are seldom close to prominent
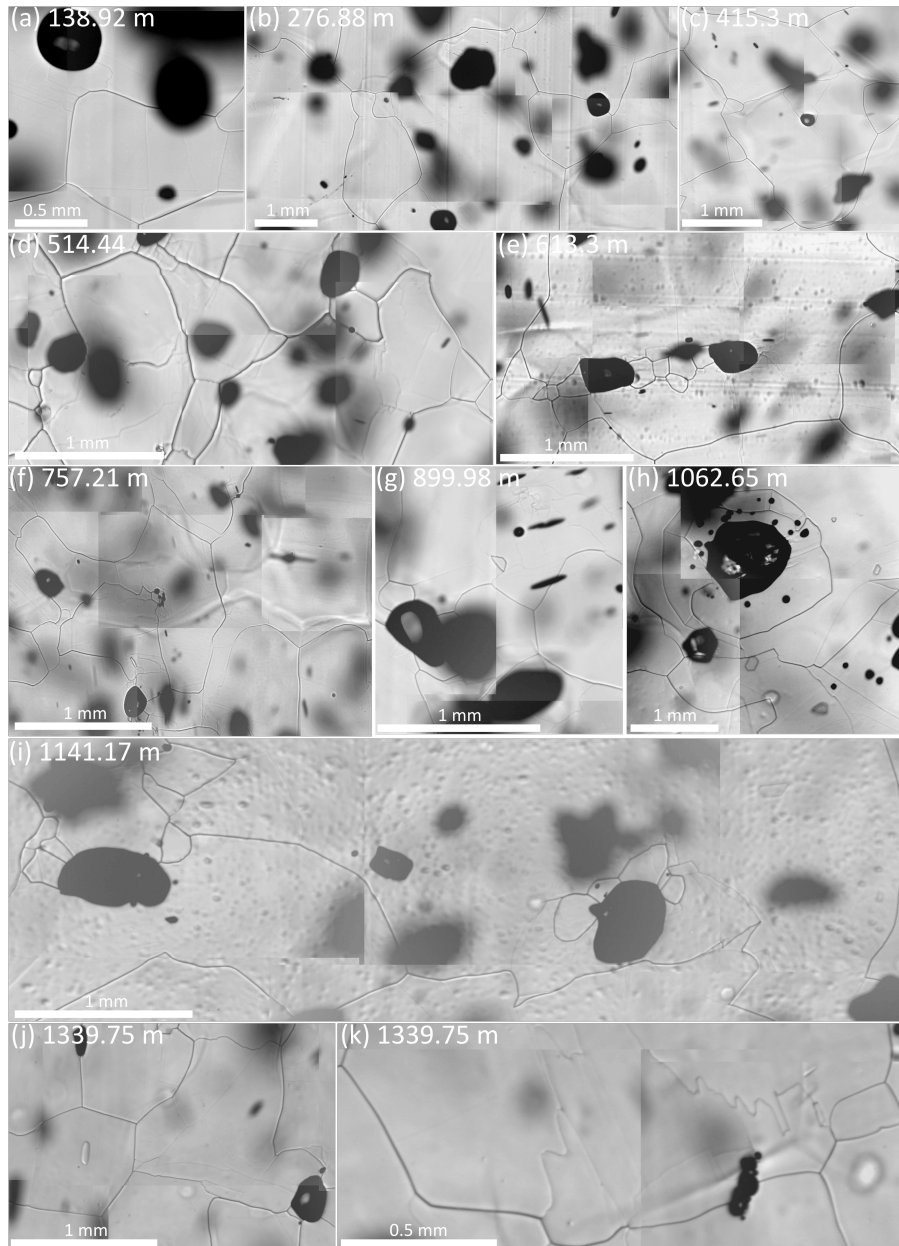
Figure 4. Features of stress, strain, and dynamic recrystallizationMicrostructural observations from all depths. Dark and grey lines are grain and subgrain boundaries, respectively. Visible are bulged and cuspidate grain boundaries (A-K), different types of subgrain boundaries (A-K), and nucleated small grains at grain boundaries (C, D, E, I, J, K). Grain boundary pinning by bubbles and subgrain boundaries (B, E, I, J) and grain islands (G) also occur. Images vary in grey values due to different light conditions, grey values of lines vary due to different depths of etch grooves.
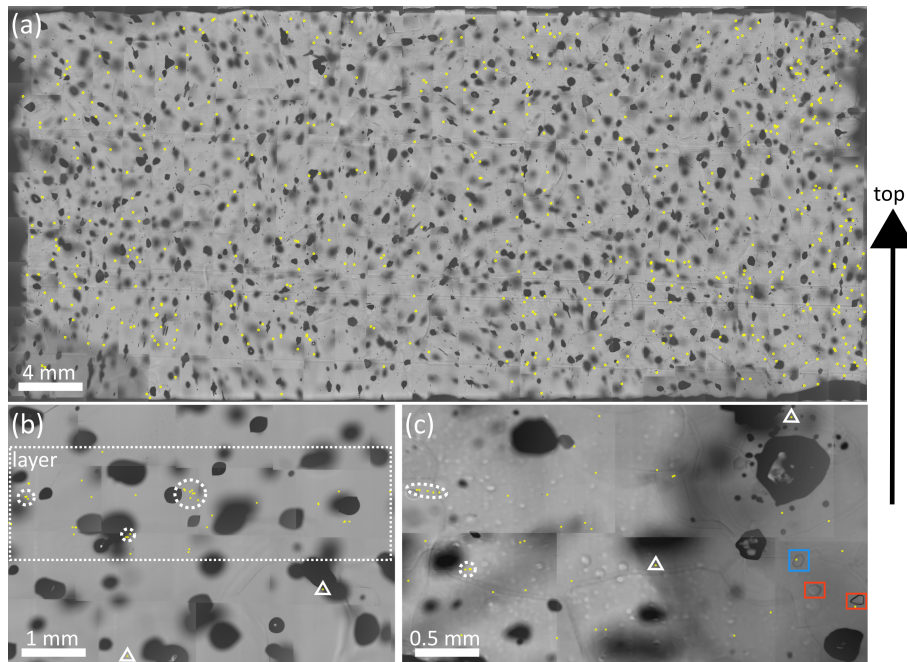
Figure 5. Locations of micro-inclusions 500 μm below the sample surface in three EGRIP samples. Annotations as in Fig. 2. White dotted circles in B) and C) indicate clusters or rows of micro-inclusions, white triangles indicate solitary micro-inclusions. Black shapes are bubbles. A) Overview of the micro-inclusions distribution at a depth of 613.3 m. Different localisation patterns can be observed, ranging from solitary inclusions to clusters of micro-inclusions (e.g., on the right side). B) Detailed section from a depth of 138.9 m. A layer of micro-inclusions, indicated by a white rectangle, accommodates clusters of micro-inclusions. C) Detailed section from a depth of 1062.65 m. Micro-inclusions are heterogeneously distributed. The blue rectangle indicates a plate-like inclusion and the red rectangles indicate clathrate hydrates.

microstructural features such as subgrain boundaries, grain islands or bulging grain boundaries. Micro-inclusions are rarely found on subgrain boundaries, which occur more often in larger grains.

3.3 Micro-inclusions at grain boundaries

3.3 Micro-inclusions in the vicinity of grain boundaries

215   1909 micro-inclusions were found in the proximity of grain boundaries, i.e. in the previously defined We analysed the impact of the chosen grain boundary thickness by applying grain boundary thicknesses of 100, 200, and 300 μm large to measure the number of micro-inclusions in the area occupied by grain boundaries (Fig. 6) . We further measured Table 1 and 2).

For 100 μm the grain boundary area varies between 6.1% (138.92 m) and 13.4% (1339.75 m) while the amount of micro-inclusions in this area varies between 5.8% (138.92 m) and 14.8% (1339.75 m) (Table 1). For 200 μm the grain
220   boundary area for all samples. varies between 11.6% (138.92 m) and 24.4% (1339.75 m) while the amount of micro-inclusions in this area varies between 14.8% (514.44 m) and 31.4% (415.3 m). This results in R_{GB} values between 0.7 (514.44 m)
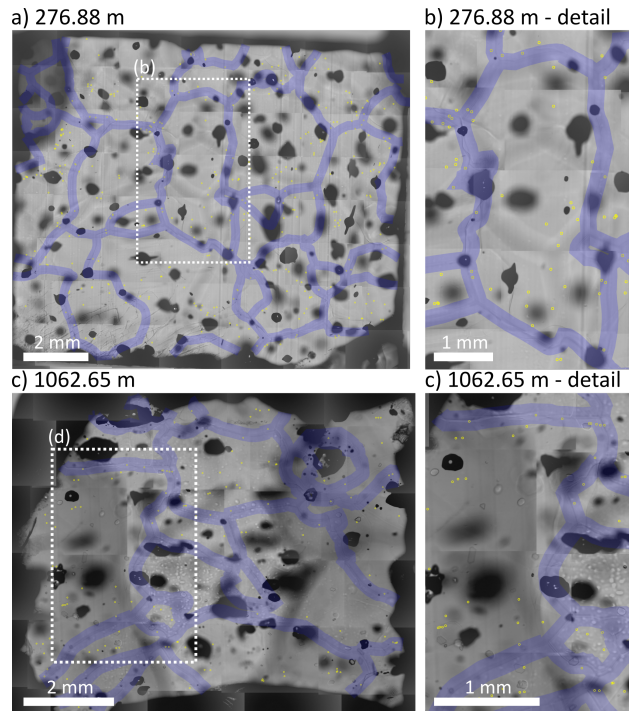
Figure 6. Samples with high R_{GB} from different depths. Note the small-scale variety in the spatial distribution of micro-inclusions in regards to grain boundaries. Annotations as in Fig. 2. a) Overview of the sample at a depth of 276.88 m with R_{GB}=1.23. Inclusions tend to cluster. b) Detail of a) showing the difference between inclusions in the grain interior (centre) and ~~at~~ in the vicinity of grain boundaries (upper left, lower right). c) Overview of the sample at a depth of 1062.65 m with R_{GB}=1.36. d) Detail of c) showing the difference between inclusions in the grain interior (left) and ~~at~~ in the vicinity of grain boundaries (upper half).

and 1.72 (415.3 m) and between 0.69 (613.3 m) and 1.78 (415.3 m) for 100 μm and 200 μm, respectively. The mean R_{GB} of all samples increases slightly with grain boundary thickness from 1.09 (100 μm) to 1.15 (200 μm).

From now on, we will always refer to a grain boundary thickness of 300 μm. 1909 micro-inclusions were found in the

225 proximity of 300 μm thick grain boundaries (Table 2 and Fig. 6). Our results are ~~upper-limit~~ an upper limit assumption since real grain boundaries are basically interfaces, with ~~an "amorphous zone " of~~ a discontinuity in lattice orientation accompanied by a zone of disorder of only a few ~~nm~~ molecule layers (Hobbs, 1974; Petrenko and Whitworth, 1999).

Between 22.3 and 42.4% of all micro-inclusions were found ~~at grain-boundaries~~ in the vicinity of grain boundaries; on average 33.3% of all micro-inclusions were ~~close to~~ in the vicinity of grain boundaries (Table 2, I_{GB}). The highest percentage of 42.4%

230 was observed in the deepest sample from 1339.75 m of depth (Bølling Allerød). Grain boundaries cover between 18.7 and 43.2% of the sample area (Table 2, A_{GB}) resulting in an average grain boundary area of 25.9%. This parameter, an ~~upper-limit~~ upper limit assumption and mainly controlled by the grain size, is close to the average value of our samples and less variable compared to the amount of micro-inclusions ~~at~~ in the vicinity of grain boundaries (Table 2, A_{GB} and I_{GB}).

Table 1. Micro-inclusions in the vicinity of grain boundaries with applied grain boundary widths of 100 and 200 μm. A_{GB} and I_{GB} were used in null hypothesis significance testing to calculate two-sided p-values.

Depth (m)	$I_{GB_{100}}$ (%)	$I_{GB_{200}}$ (%)	$A_{GB_{100}}$ (%)	$A_{GB_{200}}$ (%)	$R_{GB_{100}}$	$R_{GB_{200}}$	p-value$_{GB_{1}00}$	p-value$_{GB_{2}00}$
138.92	5.8	16.5	6.1	11.6	0.95	1.42	1.0	0.12
276.88	9.0	17.5	8.1	15.3	1.11	1.14	0.37	0.26
415.30	16	31.4	9.3	17.6	1.72	1.78	0.14	0.02
514.44	6.9	14.8	9.8	18.6	0.7	0.8	0.01	0.01
613.30	10.7	15.2	11.8	22.0	0.91	0.69	0.50	0.56
757.21	12.6	23.0	8.2	15.5	1.54	1.48	$1.74 \cdot 10^{-5}$	$1.78 \cdot 10^{-8}$
899.98	7.0	16.3	8.9	16.9	0.79	0.96	0.54	1.00
1062.65	13.5	25.6	10.4	19.3	1.3	1.33	0.25	0.08
1141.17	7.4	15.4	9.5	17.8	0.78	0.87	0.12	0.19
1339.75	14.8	30.9	13.4	24.4	1.1	1.26	0.14	0.06
-	$\emptyset\,10.37$	$\emptyset\,20.66$	$\emptyset\,9.55$	$\emptyset\,17.9$	$\emptyset\,1.09$	$\emptyset\,1.15$	$\sum 3.11 \cdot 10^{-8}$	$\sum < 2.2 \cdot 10^{-16}$

I_{GB}=percentage of micro-inclusions in the vicinity of grain boundaries, A_{GB}=accumulated area occupied by grain boundaries, R_{GB}=ratio of, X_{GB100}= grain boundary thickness of 100 μm, X_{GB200}= grain boundary thickness of 200 μm

Table 2. Samples and micro-inclusions statistics related to a grain boundary thickness of 300 μm in the upper 1340 m of the EGRIP ice core. A_{GB} and I_{GB} were used in null hypothesis significance testing to calculate two-sided p-values.

Depth (m)	Age b2k (ka)	Size Sample size (mm x mm)	n_{mi}	n_{GB}	I_{GB} (%)	A_{GB} (%)	R_{GB}	p-value
138.92	1.0	13.01 x 16.96	103	23	22.3	18.7	1.19	0.375
276.88	2.2	11.00 x 12.76	342	85	24.9	20.2	1.23	0.037
415.30	3.5	10.01 x 13.27	51	21	41.2	20.7	1.99	$8.2 \cdot 10^{-4}$
514.44	4.3	9.94 x 60.60	752	167	22.2	26.0	0.85	0.018
613.30	5.2	17.31 x 54.19	532	161	30.3	30.2	1.00	0.962
757.21	6.4	90.00 x 16.78	817	257	31.5	22.5	1.40	$3.8 \cdot 10^{-9}$
899.98	7.6	11.32 x 12.62	129	30	23.3	23.0	1.01	0.917
1062.65	9.3	9.67 x 8.47	133	46	34.6	25.5	1.36	0.022
1141.17	10.2	16.61 x 21.67	486	109	22.4	25.5	0.88	0.131
1339.75	14.1	11.24 x 11.96	2838	1010	42.4	43.2	0.98	0.549
-	-	-	$\sum 5728$	$\sum 1909$	$\emptyset\,33.3$	$\emptyset\,25.9$	$\emptyset\,1.29\ \emptyset\,1.19$	$\sum < 2.2 \cdot 10^{-16}$

n_{mi}=amount of localised micro-inclusions, n_{GB}=micro-inclusions in the vicinity of grain boundaries, I_{GB}=percentage of micro-inclusions in the vicinity of grain boundaries, A_{GB}=accumulated area occupied by grain boundaries, R_{GB}=ratio of grain boundary area to micro-inclusions in the vicinity of grain boundaries, b2k=before 2000 (Mojtabavi et al., 2020)

R_{GB}, calculated following Eq. (1), varies between 0.85 and 1.99, the mean ratio is 1.29 1.19. The lowest ratios of 0.85, 0.88 and 0.98 were found at depths of 514.44, 1141.17 and 1339.75 m, respectively. The highest ratios were 1.99, 1.40 and 1.36 at

depths of 415.3, 757.21 and 1062.65 m, respectively. The deepest sample from a depth of 1339.75 m showed the highest amount of micro-inclusions ~~at~~ in the vicinity of grain boundaries (42.4%) and the largest area occupied by grain boundaries (43.2%) as here we have the smallest grain size of all inspected samples (Fig. 1A). In general, ratios do not vary much throughout our samples and are close to 1 indicating that the relative amount of micro-inclusions ~~at~~ in the vicinity of grain boundaries is comparable at all depths. The exceptionally high ratio of 1.99 at 415.3 m is most likely caused by the low total amount of micro-inclusions (51) at this depth. Excluding this sample lowers the average R_{GB} to ~~1.2~~ 1.1.

A_{GB} and I_{GB} were used to perform null hypothesis significance testing for ten samples with an alpha of 0.05 as the cutoff for significance. If the p-value is less than 0.05, we reject the null hypothesis that micro-inclusions are preferably located ~~at~~ in the vicinity of grain boundaries and that a significant difference exists. If the p-value is larger than 0.05 no significant difference exists. Calculated p-values vary from sample to sample and range from 0.962 to $3.8 \cdot 10^{-9}$ (Table 2, p-value). Five samples have p-values below 0.05 while the other five samples have p-values above 0.05 (examples in Fig. 6). Thus, in 50% of our samples there are significantly more micro-inclusions ~~at~~ in the vicinity of grain boundaries than expected, the majority is however located in the grain interior. A small p-value often correlates with a high R_{GB} while a high p-value usually correlates with a low R_{GB}.

3.4 Identified micro-inclusions ~~at~~ in the vicinity of grain boundaries

~~A companion paper presents the results of the analysis of the mineralogy of almost 800~~ Here we present the mineralogy of micro-inclusions, identified ~~with Raman spectroscopy . Here we only present the mineralogy of micro-inclusions located at~~ (Stoll et al., 2021a), located in the vicinity of grain boundaries at all depths. In total, 181 of all identified micro-inclusions were located ~~at~~ in the vicinity of grain boundaries (i.e. 22.9%). 92 sulphate particles were found ~~at~~ in the vicinity of grain boundaries, followed by gypsum (47), quartz (28), mica (22), feldspar (21), nitrates (9), hematite (8), and titanite and anatase (both 1). 31.3% of all feldspar was found ~~at~~ in the vicinity of grain boundaries, followed by 27.6% of all gypsum , 27.2% of all mica (Table 3), 23.8% of all sulphates (including gypsum, 20.8% without gypsum), and 22.2% of all quartz.

At depths with a high diversity in sulphate types (Fig. 4, Table 2, paragraph 3.3 in ~~companion paper~~ Stoll et al. (2021a)), i.e. at 138.92, 276.88, 514.44, 613.3, 757.21, and 899.98 m, the relative amount of sulphates ~~at~~ in the vicinity of grain boundaries was higher than the relative amount of terrestrial dust, i.e. quartz, mica and feldspar. Below 900 m feldspar, mica and quartz were more common ~~at~~ in the vicinity of grain boundaries than sulphates in the form of gypsum. However, at 1339.75 m 37.9% of all identified micro-inclusions ~~at~~ in the vicinity of grain boundaries were gypsum.

4 Discussion

4.1 Evolution of grain size, microstructure and CPO at EGRIP

We briefly discuss the evolution of the mean grain size per ~~55 cm bag~~ 9 cm sample with depth, which will be analysed in more detail in a future study. The observed grain size evolution with depth is similar to findings from the NEEM ice core
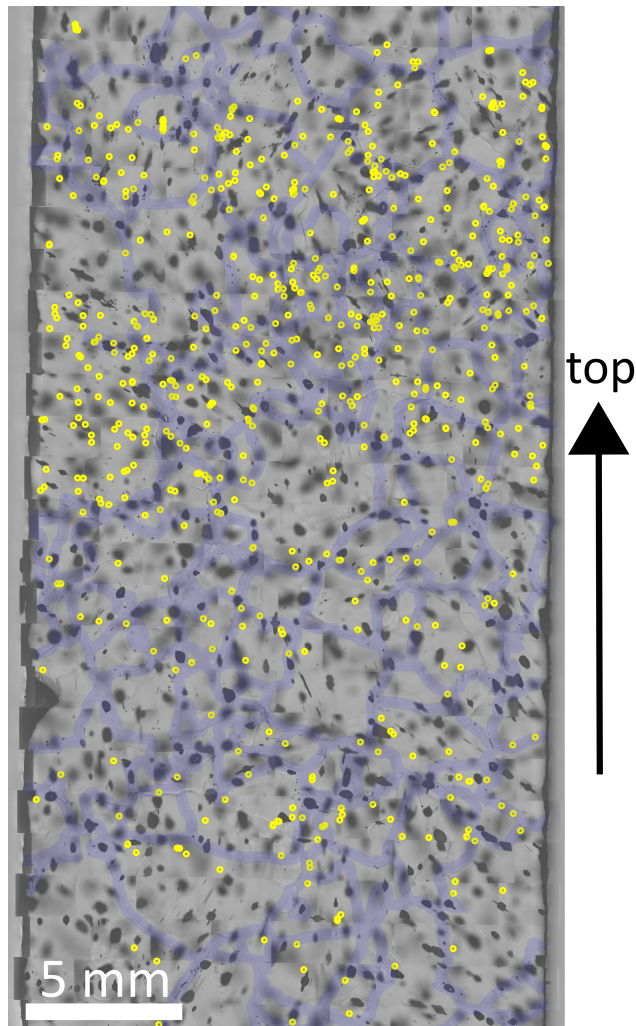
Figure 7. Locations of micro-inclusions at 757.21 m of depth. There is a cm-thick layer of inclusions in the upper half while the lower half is characterised by less inclusions and a heterogeneous distribution. Annotations as in Fig. 2.

(Eichler, 2013; Montagnat et al., 2014)(Montagnat et al., 2014) (see below), but grain size can vary highly on the centimetre-scale. The broad high variability in grain size is also displayed in the grain size distribution (Fig. 3), which also reflects the visual identification of fine grains (Fig. 1B-K). The broad distribution of grain sizes is evidence for dynamic grain growth acting via dynamic recrystallisation, a process active during or prior/after deformation. Large grains are an indicator of ordinary boundary migration recrystallization (SIBM-O) while tiny grains indicate nucleating migration recrystallization (SIBM-N) (nomenclature after Faria et al. (2014b)). Recrystallisation mechanisms are discussed in more detail in section 4.4.

A comparison with the NEEM ice core shows a similar grain size evolution with depth (Fig. 8) even though the dynamic settings are different (ice divide vs. ice stream). EGRIP grain size is generally larger in the upper 500 m and steadily
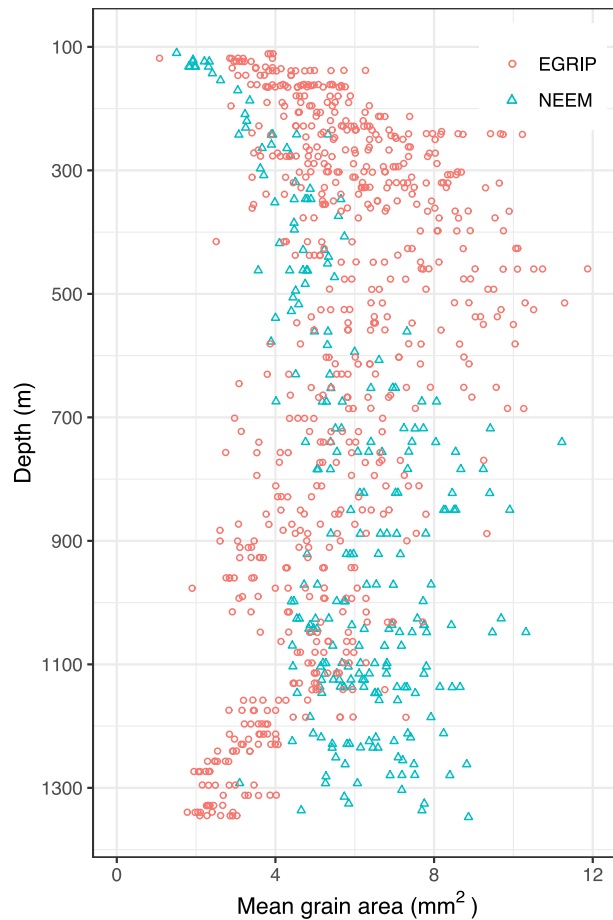
Figure 8. Grain size evolution at EGRIP and NEEM down to 1340 m. For EGRIP 9 cm section mean grain sizes derived via FA G50 are shown. NEEM data from Montagnat et al. (2014).

275 decreases below this depth. Variability between samples from similar depths is small below 1200 m. NEEM grain size increases until a depth of 740 m and is rather stable until 1350 m even though grain size variability is extreme such that is varies for several mm^2 between samples from similar depths. The cores are roughly 450 km apart, but show a similar depth-age relationship in the investigated depth range: the Glacial-Holocene transition is at 1375 m of depth at EGRIP (Mojtabavi et al., 2020) and at 1420 m at NEEM (Rasmussen et al., 2013). The ice stream thus seems to have an impact 280 on grain growth via dynamic recrystallisation in the upper several hundreds of meters. However, within the depth regime below down to the dust-loaded Glacial ice the grain size evolution seems similar to NEEM and (so far) without observable effects by the ice stream.

The broad single maximum CPO indicates a random orientation of crystals in the shallowest part of the core comparable to other ice cores, such as NEEM (Montagnat et al., 2014), European Project for Ice Coring in Antarctica in Dronning Maud

285 Land (EDML) (Weikusat et al., 2017a), and West Antarctic Ice Sheet (WAIS) (Fitzpatrick et al., 2014), and is probably the result of the just beginning vertical compression from overlying layers (Dahl-Jensen et al., 1997; Thorsteinsson et al., 1997; Faria et al., 2014b) possibly preceded by temperature gradient metamorphism (Montagnat et al., 2020). With depth, crystals rotate and basal planes shift towards the direction of extension and produce vertical girdle CPOs (Thorsteinsson et al., 1997; Wang et al., 2002). This agrees with the observed surface flow pattern of NEGIS (Fahnestock et al., 2001; Joughin et al., 2017;

290 Hvidberg et al., 2020), visual stratigraphy and CPOs measured in EGRIP thin sections from the Last Glacial (Westhoff et al., 2020). Fabric images show a diversity in c-axis orientations and enhance the girdle formation.

Microstructural features are discussed in detail in Sec. 4.4. In-depth studies on the physical properties of the EGRIP ice core will follow and are a chance to enhance our understanding of ice stream dynamics.

4.2 Localisation of micro-inclusions

4.2.1 General findings

295 We localised more than 5700 micro-inclusions within ten samples from the upper 1340 m of the EGRIP ice core. Combining optical microscopy and Raman spectroscopy confirmed that mapped micro-inclusions are indeed visible impurities below the sample surface supporting previous studies by Ohno et al. (2005, 2006); Eichler et al. (2017, 2019). The CFA data presented in a companion paper supports by Stoll et al. (2021a) support our micro-inclusion counts since CFA dust particle peaks correlate with

300 areas of highly abundant micro-inclusions.

4.2.2 Localisation as found with microstructure mapping and Raman spectroscopy

Stoll et al. (2021b) found that the observed locations of impurities in polar ice are highly diverse and results seem to be strongly influenced by the applied method. Similar to other studies applying Raman spectroscopy (e.g., Ohno et al., 2005; Sakurai et al., 2009; Eichler et al., 2017, 2019) micro-inclusions are heterogeneously distributed throughout our samples and the amount of

305 micro-inclusions close to grain boundaries varies from sample to sample. However, only a small amount of micro-inclusions is located directly on grain boundaries, the majority is located close to them. To quantitatively compare our results we calculated the ratio of micro-inclusions at in the vicinity of grain boundaries to the area of grain boundaries per sample, which reduces the impact of grain-size. Our estimates are likely too large due to the exaggerated thickness of grain boundaries, which are much smaller than 300 μm. The ratio R_{GB} oscillates around 1, which describes, on average, a coherent distribution and a

310 homogeneous spread of micro-inclusions in relation to grain boundaries throughout the core. R_{GB} tends slightly towards larger values indicating that grain boundaries may be often preferred locations of micro-inclusions . However, the are slightly more often located in the vicinity of grain boundaries than presumed from the grain boundary area. The derived p-values (Table 2, p-value) support these findingsand , but also emphasise the high variability between samples. The localisation of solid micro-inclusions seems to be much weaker than recently observed for dissolved impurities (Bohleber et al., 2020)(Bohleber et al., 2020, 2021).

Table 3. Minerals located most often in the vicinity of grain boundaries in relation to their absolute numbers and their crystal structure information in comparison to ice.

Mineral	Inclusions at GB (%)	Axial lengths (Å)	Interaxial angles (°)	Crystal system
Feldspar	31.3	a=8.290, b=12.966, c=7.151	$\alpha = 91.18, \beta = 116.31, \gamma = 90.16$	triclinic
Gypsum	27.6	a=5.674, b=15.105, c=6.491	$\alpha = 90, \beta = 118.51, \gamma = 90$	monoclinic
Mica	27.2	a=5.386, b=9.324, c=10.268	$\alpha = 90, \beta = 100.63, \gamma = 90$	trigonal
Ice 1h	-	a=4.497, b=4.497, c=7.321	$\alpha = 90, \beta = 90, \gamma = 120$	hexagonal

GB=grain boundaries, minerals at GB data from Stoll et al. (2021a), crystal structure data from Hudson Institute of Mineralogy (2021).

4.2.3 Localisation and methodology

So far, there is only a small number of studies with a comparable quantitative approach regarding impurities at in the vicinity of grain boundaries (e.g., Eichler et al., 2017). However, it must be kept in mind that optical microscopy and Raman spectroscopy only allow the detection of visible micro-inclusions. We cannot make assumptions about the locations of dissolved, i.e. invisible, impurities. Early studies (e.g., Cullen and Baker, 2000; Barnes et al., 2002b; Baker and Cullen, 2003) and recent LA-ICP-MS results by Della Lunga et al. (2017); Bohleber et al. (2020) Della Lunga et al. (2017); Bohleber et al. (2020, 2021) show that some soluble impurities, especially Na, seem to be preferably located at grain boundaries of Antarctic ice.

The sample comparison of different grain boundary thicknesses (100, 200, and 300 μm in Table 1 and Table 2) shows a similar ratio of micro-inclusion in the vicinity to grain boundaries and grain boundary area, i.e. R_{GB}, independent of the chosen grain boundary thickness or sample. This indicates that the relative number of micro-inclusions in the vicinity of grain boundaries is, on average, relatively stable and not significantly impacted by the chosen gain boundary thickness. We do not know the inclination of the grain boundaries below the surface, which supports the use of a 300 μm thick grain boundary which allows an inclination of the grain boundaries of up to 33.3°.

The sample from 1339.75 m of depth is from the Bølling Allerød, a period with dust concentrations comparable to the Last Glacial Maximum, and thus explains the high numbers of dust particles and micro-inclusions. Visual stratigraphy at this depth (Weikusat et al., 2020) already shows cloudy bands, which are characterised by fine grain size and a thus large area occupied by grain boundaries (Gow and Williamson, 1971; Svensson et al., 2005; Faria et al., 2010). These bands are probably caused by depositional events such as precipitation or sastrugi formation by redistributed surface snow (Svensson et al., 2005). Investigating those bands in detail from a microstructural and impurity perspective would help to better understand the relationship between impurity content, grain size and deformation.

Eichler et al. (2019) suggest that a higher number of micro-inclusions over a larger area should be analysed for improved statistics and more quantitative comparisons. We mostly succeeded in this approach by measuring a large total amount in micro-inclusions and, on average, more micro-inclusions per sample compared to similar studies (Ohno et al., 2005, 2006; Sakurai et al., 2010, 2011; Ohno et al., 2014). Measuring time is still an issue, especially when taking into account processes affecting the sample (e.g., sublimation). Other technical limitations are the resolution and contrast of the optics preventing the

detection of very small micro-inclusions. However, the vast majority of the total micro-inclusions should have been counted since most detectable micro-inclusions have an average diameter of 1 to 3 μm (Ruth et al., 2003; Sakurai et al., 2009; Wegner et al., 2015), and are thus within the resolution range of optical microscopes. The sample from a depth of 415.3 m has to be treated with caution. It has the highest percentage of micro-inclusions at grain-boundaries (21 of 51, i.e. 41.2%), which can be explained by the small absolute number of micro-inclusions and is thus, most likely a statistical outlier. The comparably small area occupied by grain-boundaries (20.0%) further supports the possibility of an outlier and a biased statistics caused by the small total amount of micro-inclusions in this sample.

4.2.4 Localisation of micro-inclusions at different depths

We rarely observed distinct horizontal bands of micro-inclusions except at a depth of 757 m (Fig. 7). 7-11% of all micro-inclusion micro-inclusions in EDML ice analysed by Eichler et al. (2017) were at in the vicinity of grain boundaries, these samples are from the early Eeminan (MIS 5.5), i.e. "warm period ice", and thus comparable to our Holocene samples. Their NEEM samples showed a more spread-out distribution across the samples, and between 18 and 24% of micro-inclusions were at in the vicinity of grain boundaries. This supports our findings (22-41% at in the vicinity of grain boundaries) in EGRIP Holocene ice even though our values are generally higher. Eichler et al. (2017) analysed NEEM samples from a depth of 739.9 and 740.2 m, which is close to our samples from 613.3 and 757.21 m of depth with values of 30.3 and 31.5 %, respectively. Our higher value can be explained by sample selection from depths with high dust content as shown in a companion paper. Our results indicate that the spatial variability of micro-inclusions within Holocene ice is larger than previously thought emphasising the difficulty in generalising spatial patterns as suggested by Stoll et al. (2021b).

Summarising, our observations regarding the location of micro-inclusions show that the spatial variability is very high and changes on the millimetre- to centimetre-scale. Thus, generalisations about the location of micro-inclusions should be made with care and have to be specified for the depth intervals considered. However, the majority of micro-inclusions is found in the grain interior even though grain boundaries at some depths locate comparably high numbers of micro-inclusions. Interestingly, we were not able to link physical properties of the ice, such as grain size and CPO, to distinct distributional patterns of micro-inclusions. Investigating these relationships remains challenging due to e.g., 1) the different sizes of ice grains and samples and 2) the heterogeneity in grain size and micro-inclusion distribution on the mm to cm-scale. We thus suggest in-depth investigations of cloudy bands for future research.

4.3 Impact of micro-inclusions on ice properties

Impurities affect the physical and mechanical properties of ice, especially the deformation and the flow of ice (Paterson, 1991; Cullen and Baker, 2001), and most studies show that impurity-rich ice is easier to deform than impurity-poor ice (e.g., Fisher and Koerner, 1986; Paterson, 1991; Cuffey et al., 2000). The potential influence of impurities on other, partly related, ice properties, such as CPO and grain size, are complex and manifold (Stoll et al., 2021b). We discuss potential processes involving micro-inclusions and observed microstructural features and their implications for deformation via dominant mechanisms, and dynamic recrystallization.

Zener pinning and drag of grain boundaries by impurities are suggested to be major mechanisms impacting grain size (e.g., Smith, 1948; Alley et al., 1986a; Fisher and Koerner, 1986; Alley and Woods, 1996; Paterson, 1991; Weiss et al., 2002; Durand et al., 2006). Even though roughly one third of all mapped micro-inclusions were located in proximity (300 μm upper limit assumption) to grain boundaries (Table 2), we did not observe any direct indications of micro-inclusions involved in Zener pinning or drag. Direct indications would be e.g., a sharp edge at a second phase particle in an otherwise curved grain boundary segment or a bulging grain boundary restricted by a second phase particle (e.g., Fig. 2 in Stoll et al. (2021b)) (Passchier and Trouw, 2005). This agrees with other studies (Ohno et al., 2005; Faria et al., 2010; Eichler et al., 2017, 2019) and indicates that the grain evolution is not affected strongly by the strict Zener pining process of micro-inclusions as proposed by Alley et al. (1986b), but if effected affected via reduced grain growth at all, it may rather be effected affected by a reduced grain boundary mobility. Fisher and Koerner (1986); Alley et al. (1986b); Li et al. (1998); Iliescu and Baker (2008) suggest that impurity concentrations must be above a threshold to result in counteracted grain boundary mobility and restricted grain growth by Zener pinning. However, quantitative thresholds are vaguely defined and partly ambiguous and thus difficult to discuss. It is possible that EGRIP Holocene dust concentrations are below this vague threshold to impact grain size development significantly via pining, but unlikely because we also analysed samples comparable to Glacial ice, i.e. with high dust concentrations (discussed in a companion paper) and small grains (e.g., Fig. 1J and K). However, to confirm this assumption, a larger number of samples from the glacial period must be analysed.

High impurity layers showed no microstructural evidence for grain boundary sliding, such as linked-up grain boundaries or rectangular and lath-shaped grains (Fig. 6 in Goldsby and Kohlstedt (1997), Fig. 2B in Kuiper et al. (2020b)). Our results (Fig. 4) indicate that solid micro-inclusions are not a main driver of do not have a major impact on the grain size evolution by e.g., grain size change via enhancing the gradients of internal strain energies due to localised deformation along grain boundaries. However, it is possible that further methodological progress is needed to directly identify the impact of solid inclusions on grain size and potential localised deformation via other deformation mechanisms e.g., Frank-Read sources and the multiplication and entanglement of dislocations, heterogeneous strain distribution within grains or dislocation pile-up on inclusions representing glide obstacles (Frank and Read, 1950; Ahmad et al., 1986; Weertman and Weertman, 1992).

The localisation of micro-inclusions at in the vicinity of grain boundaries in our samples seems to be somewhat related to their mineralogy (Table 3, Fig. 8 in companion paper). In the case of solid micro-inclusions the interface properties between the ice and the particle play a crucial role and are thus probably influenced by the mineralogy and thus the surface properties of the inclusion at a grain boundary. We know from anti-freeze proteins (e.g., Bayer-Giraldi et al., 2018) that "ice-binding" properties result from similar surface structures (on the crystal lattice scale) of the second phase particle and the ice crystal. Less than one third of all feldspar, gypsum, and mica inclusions were located at in the vicinity of grain boundaries, which is in good agreement with our average derived percentage of micro-inclusions at in the vicinity of grain boundaries. These minerals have partly comparable crystallographic lattice parameters to ice Ih (Table 3). Especially the properties of feldspar are similar, or multiples, to the properties of ice while the crystallographic properties of gypsum and mica are less similar. Fenter et al. (2000) show that, after removing the outermost K ions, remaining Si atoms of K-rich feldspars become attached to OH or O resulting in a surface prone to interact with water molecules via hydrogen bonding. In addition, electrostatic interactions between the

feldspar surface and the dipole moment of water might be enabled by the charged crystal lattice of feldspars (Yakobi-Hancock et al., 2013). Investigating the impact of these crystallographic properties in depth goes beyond the scope of this study, but might be of interest for future studies.

While Bohleber et al. (2020) found element-specific localisation trends for dissolved impurities we show that it is more complex for solid micro-inclusions. While the composition of the micro-inclusions may play a certain role, as explained above, it seems to become clear that its state, i.e. solid, is more important especially when compared to studies on dissolved impurities (e.g., Bohleber et al., 2020). Bohleber et al. (2020) show that Na^+ intensity peaks at grain boundaries, as proposed by e.g., Barnes and Wolff (2004), which supports the probable difference between dissolved and undissolved impurities (Stoll et al., 2021b). A comparison of different methods by analysing the same samples is thus of great interest to clarify the role of the 1) state of impurities and 2) of the applied method. With respect to the interface processes mentioned above, another aspect is the poorly understood structure of grain boundaries in ice. The density anomaly of water, in contrast to metals or minerals, leads to molecules in grain boundaries being packed more closely than in the lattice and amorphous water veins, which can be either liquid-like (e.g., Mader, 1992) or solid-like), thus exist at grain boundaries (Azuma et al., 2012). Depending on the conditions, mainly changed change in temperature, but possibly also pressure and salt content, these veins can become liquid-like and thus allow premelting and "slippery" grain boundaries as suspected by Kuiper et al. (2020a). Comparably Comparable to air bubbles during normal grain growth, dissolved impurities are mobile enough to interact and affix on migrating grain boundaries (Azuma et al., 2012), thus influencing their migration mobility. The concentration of dissolved impurities at grain boundaries could thus increase with time resulting eventually in a decreasing grain boundary mobility. Azuma et al. (2012) observed an increase in the number of air bubbles at grain boundaries with time, the possibility of a time-dependent concentration of dissolved impurities at grain boundaries should thus be investigated in detail with an appropriate method, such as LA-ICP-MS. That solid inclusions, in an almost constant temperature regime, do not tend to affix to grain boundaries, is indicated by our finding that the relative amount of mineral particles found at grain boundaries does not change significantly with depth (Table 2).

Deforming ice might enable palaeorecord alteration and enhance impurities to change locations with time and thus, mix and react in ice as discussed in detail in a companion paper and suggested by e.g., Masson-Delmotte et al. (2010); Faria et al. (2010); de Angelis et al. (2013); Baccolo et al. (2018). Migrating grain boundaries, driven by grain growth and dynamic recrystallization, could transport dissolved accumulated impurities, which eventually react, form and precipitate as salt micro-particles. Furthermore, impurities located in shear bands, which undergo high strain might lead to increased mechanical mixing rates (Eichler et al., 2019). Our study supports the possibility of such reactions occurring already in comparably shallow ice. The post depositional movement of sulphate ions suggested by Barnes et al. (2003); de Angelis et al. (2013) could explain the high frequency of clusters (Fig. 5). In deep Vostok ice de Angelis et al. (2005) observed the relocation of mineral particles in large clusters related to grain boundary migration during extreme grain growth conditions. Our samples are from a different temperature regime and not from bottom ice and processes, such as abnormal grain growth, thus do not take place, but the overall mechanisms could be similar and should be investigated further. de Angelis et al. (2013) suggest that in EPICA Dome C bottom ice acid-salt interactions, ion relocation and salt formation occur in situ in relation with ice recrystallization, but secondary salt formation is

limited to acids relocated at grain boundaries at the surface of primary salts in inclusions. A large inclusion (~800 μm) analysed with high resolution synchrotron X-Ray micro-fluorescence was a complex structure containing a variety of minerals and tens of particle aggregates formed by gathering and mixing of several liquid phases and solid particles (de Angelis et al., 2013). Oversaturation in residual pockets containing carbonate and calcium ions resulted in the precipitation of calcium carbonate. The observation that micro-inclusions in our samples, especially sulphates, form clusters indicates that these processes have to be considered in EGRIP ice as well. Such detailed investigations are very valuable, but highly complex and costly and thus not suitable for extensive studies on micro-inclusions at several depths of one ice core as aimed for in this study.

4.4 Microstructural indications of recrystallization and deformation

Apart from direct impurity effects there are also indirect effects which could have an influence on the grain size development and the microstructure of our samples. Grain shape and grain size are both also a product of recrystallization processes, such as rotation recrystallization, strain-induced boundary migration with or without nucleation, and normal grain growth. Nucleating migration recrystallization (SIBM-N) involves the formation of new grain boundaries, if no new grains are formed ordinary boundary migration recrystallization (SIBM-O) takes place (nomenclature after Faria et al. (2014b))(Faria et al., 2014b). Indications of recrystallization processes, such as abundant subgrain boundaries, grain islands and bulging grain boundaries, were observed at all depths (Fig. 4) and indicate dynamic recrystallisation during deformation (in contrast to static recrystallization occurring without or after deformation) (Passchier and Trouw, 2005). Subgrain boundaries are stable structures of localised distortions of the lattice (Faria et al., 2014b). The vast occurrence of subgrain boundaries indicates internal stresses, heterogeneous strains, and high dislocation densities, which result in the arrangement of dislocations in arrays (polygonization after Poirier (1985)) and can be interpreted as early stages of rotation recrystallization (Drury and Urai, 1990) leading to the formation of new grain boundaries. All three subgrain boundary types (normal, parallel, zigzag) described by Weikusat et al. (2009) were observed at all depths (Fig. 4) indicating a high mechanical anisotropy. Electron Backscatter Diffraction or X-ray Laue diffraction would be needed to identify possible active slip systems of the dislocations in our samples (Piazolo et al., 2008; Weikusat et al., 2011, 2017b; Chauve et al., 2017). In analogy to previous results from polar ice (NEEM, EDML) the high abundance of subgrain boundaries parallel to the basal plane could be basal twist boundaries, but also have the potential that internal stresses are sufficient to also produce non-basal dislocations. However, rotation axes data are needed to verify this for EGRIP. Furthermore, the grain boundary shapes indicates indicate strain-induced boundary migration driven by different dislocation densities in neighbouring grains and thus the bulging of grain boundaries into grains with higher strain energy (Weertman and Weertman, 1992; Humphreys and Hatherly, 2004). At the same depth, i.e. under similar boundary conditions, fewer fine grains undergo subgrain boundary formation than larger grains. Weikusat et al. (2009) observed the same for EDML ice and suggested that subgrain formation is not related to different shear behaviour, which is often attributed to a high impurity content (Paterson, 1991). Accepting recrystallization as the major grain size control a possible interpretation of varying grain size with varying impurity load can be found in the recrystallization diagram suggested by Faria et al. (2014b): recrystallization processes, in their sum, dictated by the given boundary conditions (pressure or strain rate and temperature) lead to a "steady state grain size" (Steinbach et al., 2017), in rock-forming minerals characterised as stress dependent (paleo-piezometer, e.g., Karato et al.

(1980); Rutter (1995); Stipp and Tullis (2003)), and possibly reflected by observations (e.g., Jacka and Li, 1994; Treverrow et al., 2012). Impurity load is another boundary control and can move the "ground level" of the steady state grain size. Thus, under macroscopic conditions (pressure, temperature, strain rate) another (smaller) steady state grain size would be reached by the system. The process behind may be the changed mix of recrystallization processes, or the changed grain boundary mobility by impurity load (see above).

The observed microstructure (Fig. 4) indicates dynamic recrystallization and thus active deformation by dislocation activity throughout the upper 1340 m of the EGRIP ice core. Active deformation probably continues with depth due to similar deformation mechanisms taking place below 1340 m as indicated by vertical girdle CPOs (Westhoff et al., 2020). Dynamic recrystallization does not act only at specific depth regimes, but throughout the ice column as was observed in other deep ice cores from less dynamic sites (e.g., Durand et al., 2008; Weikusat et al., 2009; Faria et al., 2014b). A dedicated study on the microstructure throughout the EGRIP ice core, analysing a larger amount of samples, is however needed to investigate the internal mechanisms taking place in detail.

5   Conclusions

We here derive the first systematic analysis of the microstructural location of micro-inclusions in Holocene and Late Glacial ice from the EGRIP ice core, the first deep ice core from a fast flowing ice stream. The analysis of grain size, CPO and microstructural features along the core was accompanied by an investigation of the locations of micro-inclusions in with respect to grain boundaries. The spatial distribution of micro-inclusions is highly diverse, and strongly depends on the applied scale. Micro-inclusions are found in centimetre-thick layers, in local clusters and rows, and in solitariness. We quantify the relationship between micro-inclusions and grain boundaries and show that roughly two-thirds of all micro-inclusions are located in the grain interior. However, in half of all samples, grain boundaries are slightly preferred locations, but never in a vast extent. However, no more preferred locations than presumed from the grain boundary area. No significant relationship between depth and micro-inclusion distribution in relation to the microstructure was found. The combination of optical microscopy and Cryo-Raman spectroscopy data showed shows that minerals, such as feldspar, seem to be more likely to be located at in the vicinity of grain boundaries which could be caused by the interface properties due to their crystallographic structures, inclusion-ice interface properties or the structure of grain boundaries in ice.

Extensional deformation is the dominant deformation regime in our samples. However, no direct effects of micro-inclusions on the microstructure, such as typical local pinning microstructures, were observed. Observed clustering of micro-inclusions could indicate post depositional movement of micro-inclusions, which would imply possible effects on ice crystals already at shallow depths. All samples showed extensive implications of dynamic recrystallization, such as bulging grains, grain islands and different types of subgrain boundaries implying high internal strains and stresses, but no direct link to the location of the micro-inclusions. Grain boundary mobility is possibly reduced (overall not locally) by dissolved impurities, changing interface properties or the grain boundary structure impacted by impurities. Observing and defining the impact of impurities on the deformation of ice continues to be a challenge, which might need new methodological approaches. Our systematic overview

510 of micro-inclusions throughout a large part of one ice core is a step forward towards more holistic impurity and microstructure studies, and thus a better understanding of the physical properties of polar ice.

Data availability. High-resolution impurity maps and CPO data are available at PANGAEA. Grain size data on PANGAEA is being updated.

Author contributions. Conceptualisation by NS, IW, and MH. Microstructure mapping and Raman methodology developed by NS, JE, and IW. Investigation and data curation by NS. Formal analysis by NS and TE. Funding acquisition for NS by IW. The original draft was written
515 by NS with assistance from all co-authors.

Competing interests. The authors declare that the research was conducted in the absence of any commercial or financial relationships that could be construed as a potential conflict of interest.

Acknowledgements. This work was carried out as part of the Helmholtz Junior Research group "The effect of deformation mechanisms for ice sheet dynamics" (VH-NG-802). We especially thank the EGRIP physical properties team, e.g., Johanna Kerch, Ina Kleitz, Daniela
520 Jansen, Sebastian Hellmann, Wataru Shigeyama, Julien Westhoff, Ernst-Jan Kuiper, Tomoyuki Homma, Steven Franke and David Wallis. We also thank all other EGRIP participants for logistical support, ice processing and fruitful discussions. EGRIP is directed and organised by the Centre for Ice and Climate at the Niels Bohr Institute, University of Copenhagen. It is supported by funding agencies and institutions in Denmark (A. P. Møller Foundation, University of Copenhagen), USA (US National Science Foundation, Office of Polar Programs), Germany (Alfred Wegener Institute, Helmholtz Centre for Polar and Marine Research), Japan (National Institute of Polar Research and
525 Arctic Challenge for Sustainability), Norway (University of Bergen and Trond Mohn Foundation), Switzerland (Swiss National Science Foundation), France (French Polar Institute Paul-Emile Victor, Institute for Geosciences and Environmental research), Canada (University of Manitoba) and China (Chinese Academy of Sciences and Beijing Normal University). TE and CMJ gratefully acknowledge the long-term financial support of ice core research at the University of Bern by the Swiss National Science Foundation (grant no. 200020_172506 (iCEP) and 20FI21_164190 (EGRIP)).

References

Ahmad, S., Ohtomo, M., and Whitworth, R. W.: Observation of a dislocation source in ice by synchrotron radiation topography, Nature, 319, 659–660, https://doi.org/10.1038/319659a0, https://doi.org/10.1038/319659a0http://www.nature.com/articles/319659a0, 1986.

Alley, R., Perepezko, J., and Bentley, C. R.: Grain Growth in Polar Ice: I. Theory, Journal of Glaciology, 32, 415–424, https://doi.org/10.3189/S0022143000012132, 1986a.

Alley, R. B.: Fabrics in polar ice sheets: Development and prediction, Science, 240, 493–495, https://doi.org/10.1126/science.240.4851.493, 1988.

Alley, R. B. and Woods, G. A.: Impurity influence on normal grain growth in the GISP2 ice core, Greenland, Journal of Glaciology, 42, 255–260, 1996.

Alley, R. B., Blankenship, D. D., Bentley, C. R., and Rooney, S. T.: Deformation of till beneath ice stream B, West Antarctica, Nature, 322, 57, https://doi.org/10.1038/322057a0http://10.0.4.14/322057a0, 1986b.

Alley, R. B., Blankenship, D. D., Rooney, S. T., and Bentley, C. R.: Water-pressure coupling of sliding and bed deformation: III. Application to Ice Stream B, Antarctica, Journal of Glaciology, 35, 1989.

Ashby, M. F.: Boundary defects and the mechanism of particle movement through crystals, Scripta Metallurgica, 3, 843–848, https://doi.org/https://doi.org/10.1016/0036-9748(69)90192-6, 1969.

Azuma, N., Miyakoshi, T., Yokoyama, S., and Takata, M.: Impeding effect of air bubbles on normal grain growth of ice, Journal of Structural Geology, 42, 184–193, https://doi.org/10.1016/j.jsg.2012.05.005, 2012.

Baccolo, G., Cibin, G., Delmonte, B., Hampai, D., Marcelli, A., Stefano, E. D., Macis, S., and Maggi, V.: The Contribution of Synchrotron Light for the Characterization of Atmospheric Mineral Dust in Deep Ice Cores : Preliminary Results from the Talos Dome Ice Core (East Antarctica), Condensed Matter, 3, https://doi.org/10.3390/condmat3030025, 2018.

Baker, I. and Cullen, D.: SEM/EDS observations of impurities in polar ice: artifacts or not?, Journal of Glaciology, 49, 184–190, 2003.

Barnes, P. R. F. and Wolff, E. W.: Distribution of soluble impurities in cold glacial ice, Journal of Glaciology, 50, 311–324, https://doi.org/10.3189/172756504781829918, 2004.

Barnes, P. R. F., Mulvaney, R., Robinson, K., and Wolff, E. W.: Observations of polar ice from the Holocene and the glacial period using the scanning electron microscope, Annals of Glaciology, 35, 559–566, 2002a.

Barnes, P. R. F., Mulvaney, R., Wolff, E. W., and Robinson, K.: A technique for the examination of polar ice using the scaning electron microscope, Journal of Microscopy, 205, 118–124, 2002b.

Barnes, P. R. F., Wolff, E. W., Mader, H. M., Udisti, R., Castellano, E., and Röthlisberger, R.: Evolution of chemical peak shapes in the Dome C, Antarctica, ice core, Journal of Geophysical Research, 108, 4126, https://doi.org/10.1029/2002JD002538, 2003.

Bayer-Giraldi, M., Sazaki, G., Nagashima, K., Kipfstuhl, S., Vorontsov, D. A., and Furukawa, Y.: Growth suppression of ice crystal basal face in the presence of a moderate ice-binding protein does not confer hyperactivity, Proceedings of the National Academy of Sciences, 115, 7479–7484, https://doi.org/10.1073/pnas.1807461115, 2018.

Bohleber, P., Roman, M., Šala, M., and Barbante, C.: Imaging the impurity distribution in glacier ice cores with LA-ICP-MS, Journal of Analytical Atomic Spectrometry, https://doi.org/10.1039/d0ja00170h, 2020.

Bohleber, P., Roman, M., Šala, M., Delmonte, B., Stenni, B., and Barbante, C.: Two-dimensional impurity imaging in deep Antarctic ice cores: snapshots of three climatic periods and implications for high-resolution signal interpretation, The Cryosphere, 15, 3523–3538, https://doi.org/10.5194/tc-15-3523-2021, https://tc.copernicus.org/articles/15/3523/2021/, 2021.

Chauve, T., Montagnat, M., Piazolo, S., Journaux, B., Wheeler, J., Barou, F., Mainprice, D., and Tommasi, A.: Non-basal dislocations should be accounted for in simulating ice mass flow, Earth and Planetary Science Letters, 473, 247–255, https://doi.org/10.1016/j.epsl.2017.06.020, 2017.

570 Cole-Dai, J., Budner, D. M., and Ferris, D. G.: High Speed, High Resolution, and Continuous Chemical Analysis of Ice Cores Using a Melter and Ion Chromatography, Environmental Science & Technology, 40, 6764–6769, https://doi.org/10.1021/es061188a, 2006.

Cuffey, K. M., Conway, H., Gades, A., Hallet, B., Raymond, C. F., and Whitlow, S.: Deformation properties of subfreezing glacier ice : Role of crystal size , chemical impurities , and rock particles inferred from in situ measurements, Journal of Geophysical Research, 105, 27 895–27 915, 2000.

575 Cullen, D. and Baker, I.: The chemistry of grain boundaries in Greenland ice, Journal of Glaciology, 46, 703–706, 2000.

Cullen, D. and Baker, I.: Observation of Impurities in Ice, Microscopy Research and Technique, 207, 198–207, 2001.

Dahl-Jensen, D. and Gundestrup, N. S.: Constitutive properties of ice at Dye 3, Greenland, International Association of Hydrological Sciences Publication, pp. 31–43, http://hydrologie.org/redbooks/a170/iahs_170_0031.pdf, 1987.

Dahl-Jensen, D., Thorsteinsson, T., Alley, R., and Shoji, H.: Flow properties of the ice from the Greenland Ice Core Project ice core: The
580 reason for folds?, Journal of Geophysical Research: Oceans, 102, 26 831–26 840, https://doi.org/10.1029/97JC01266, 1997.

Dahl-Jensen, D., Albert, M. R., Aldahan, A., Azuma, N., Balslev-Clausen, D., Baumgartner, M., Berggren, A. M., Bigler, M., Binder, T., Blunier, T., Bourgeois, J. C., Brook, E. J., Buchardt, S. L., Buizert, C., Capron, E., Chappellaz, J., Chung, J., Clausen, H. B., Cvijanovic, I., Davies, S. M., Ditlevsen, P., Eicher, O., Fischer, H., Fisher, D. A., Fleet, L. G., Gfeller, G., Gkinis, V., Gogineni, S., Goto-Azuma, K., Grinsted, A., Gudlaugsdottir, H., Guillevic, M., Hansen, S. B., Hansson, M., Hirabayashi, M., Hong, S., Hur, S. D., Huybrechts, P.,
585 Hvidberg, C. S., Iizuka, Y., Jenk, T., Johnsen, S. J., Jones, T. R., Jouzel, J., Karlsson, N. B., Kawamura, K., Keegan, K., Kettner, E., Kipfstuhl, S., Kjær, H. A., Koutnik, M., Kuramoto, T., Köhler, P., Laepple, T., Landais, A., Langen, P. L., Larsen, L. B., Leuenberger, D., Leuenberger, M., Leuschen, C., Li, J., Lipenkov, V., Martinerie, P., Maselli, O. J., Masson-Delmotte, V., McConnell, J. R., Miller, H., Mini, O., Miyamoto, A., Montagnat-Rentier, M., Mulvaney, R., Muscheler, R., Orsi, A. J., Paden, J., Panton, C., Pattyn, F., Petit, J. R., Pol, K., Popp, T., Possnert, G., Prié, F., Prokopiou, M., Quiquet, A., Rasmussen, S. O., Raynaud, D., Ren, J., Reutenauer, C., Ritz, C.,
590 Röckmann, T., Rosen, J. L., Rubino, M., Rybak, O., Samyn, D., Sapart, C. J., Schilt, A., Schmidt, A. M., Schwander, J., Schüpbach, S., Seierstad, I., Severinghaus, J. P., Sheldon, S., Simonsen, S. B., Sjolte, J., Solgaard, A. M., Sowers, T., Sperlich, P., Steen-Larsen, H. C., Steffen, K., Steffensen, J. P., Steinhage, D., Stocker, T. F., Stowasser, C., Sturevik, A. S., Sturges, W. T., Sveinbjörnsdottir, A., Svensson, A., Tison, J. L., Uetake, J., Vallelonga, P., Van De Wal, R. S., Van Der Wel, G., Vaughn, B. H., Vinther, B., Waddington, E., Wegner, A., Weikusat, I., White, J. W., Wilhelms, F., Winstrup, M., Witrant, E., Wolff, E. W., Xiao, C., and Zheng, J.: Eemian interglacial reconstructed
595 from a Greenland folded ice core, Nature, 493, 489–494, https://doi.org/10.1038/nature11789, 2013.

de Angelis, M., Morel-Fourcade, M.-C., Barnola, J.-M., Susini, J., and Duval, P.: Brine micro-droplets and solid inclusions in accreted ice from Lake Vostok (East Antarctica), Geophysical Research Letters, 32, n/a–n/a, https://doi.org/10.1029/2005GL022460, 2005.

de Angelis, M., Tison, J. L., Morel-Fourcade, M. C., and Susini, J.: Micro-investigation of EPICA Dome C bottom ice: Evidence of long term in situ processes involving acid-salt interactions, mineral dust, and organic matter, Quaternary Science Reviews, 78, 248–265,
600 https://doi.org/10.1016/j.quascirev.2013.08.012, 2013.

Della Lunga, D., Müller, W., Rasmussen, S. O., and Svensson, A.: Location of cation impurities in NGRIP deep ice revealed by cryo-cell UV-laser-ablation ICPMS, Journal of Glaciology, 60, 970–988, https://doi.org/10.3189/2014JoG13J199, 2014.

Della Lunga, D., Müller, W., Rasmussen, S. O., Svensson, A., and Vallelonga, P.: Calibrated cryo-cell UV-LA-ICPMS elemental concentrations from the NGRIP ice core reveal abrupt, sub-annual variability in dust across the GI-21.2 interstadial period, The Cryosphere, 11, 1297–1309, https://doi.org/10.5194/tc-11-1297-2017, 2017.

Drury, M. R. and Urai, J. L.: Deformation-related recrystalization processes, Tectonophysics, 172, 235–253, 1990.

Durand, G., Gagliardini, O., Thorsteinsson, T., Svensson, A., Kipfstuhl, S., and Dahl-Jensen, D.: Ice microstructure and fabric: an up-to-date approach for measuring textures, Journal of Glaciology, 52, 619–630, 2006.

Durand, G., Persson, A., Samyn, D., and Svensson, A.: Relation between neighbouring grains in the upper part of the NorthGRIP ice core - Implications for rotation recrystallization, Earth and Planetary Science Letters, 265, 666–671, https://doi.org/10.1016/j.epsl.2007.11.002, 2008.

Eichler, J.: C-axis analysis of the NEEM ice core: an approach based on digital image processing, Ph.D. thesis, Freie Universität Berlin, Berlin, 2013.

Eichler, J., Kleitz, I., Bayer-Giraldi, M., Jansen, D., Kipfstuhl, S., Shigeyama, W., Weikusat, C., and Weikusat, I.: Location and distribution of micro-inclusions in the EDML and NEEM ice cores using optical microscopy and in situ Raman spectroscopy, Cryosphere, 11, 1075–1090, https://doi.org/10.5194/tc-11-1075-2017, 2017.

Eichler, J., Weikusat, C., Wegner, A., Twarloh, B., Behrens, M., Fischer, H., Hörhold, M., Jansen, D., Kipfstuhl, S., Ruth, U., Wilhelms, F., and Weikusat, I.: Impurity Analysis and Microstructure Along the Climatic Transition From MIS 6 Into 5e in the EDML Ice Core Using Cryo-Raman Microscopy, Frontiers in Earth Science, 7, 1–16, https://doi.org/10.3389/feart.2019.00020, 2019.

EPICA Community Members: Eight glacial cycles from an Antarctic ice core EPICA community members, Nature, 429, 623–628, 2004.

Fahnestock, M., Abdalati, W., Joughin, I., Brozena, J., and Gogineni, P.: High Geothermal Heat Flow, Basal Melt, and the Origin of Rapid Ice Flow in Central Greenland, Science, 294, 2338 LP – 2342, https://doi.org/10.1126/science.1065370, 2001.

Faria, S. H., Freitag, J., and Kipfstuhl, S.: Polar ice structure and the integrity of ice-core paleoclimate records, Quaternary Science Reviews, 29, 338–351, https://doi.org/10.1016/j.quascirev.2009.10.016, 2010.

Faria, S. H., Weikusat, I., and Azuma, N.: The microstructure of polar ice. Part I: Highlights from ice core research, Journal of Structural Geology, 61, 2–20, https://doi.org/10.1016/j.jsg.2013.09.010, 2014a.

Faria, S. H., Weikusat, I., and Azuma, N.: The microstructure of polar ice. Part II: State of the art, Journal of Structural Geology, 61, 21–49, https://doi.org/10.1016/j.jsg.2013.11.003, 2014b.

Fenter, P., Teng, H., Geissbühler, P., Hanchar, J., Nagy, K., and Sturchio, N.: Atomic-scale structure of the orthoclase (001)–water interface measured with high-resolution X-ray reflectivity, Geochimica et Cosmochimica Acta, 64, 3663–3673, https://doi.org/10.1016/S0016-7037(00)00455-5, 2000.

Fisher, B. D. A. and Koerner, R. M.: On The special Rheological Properties of ancient Microparticles-laden Northern Hemisphere Ice as derived from Borehole and Core Measurements, Journal of Glaciology, 32, 501–510, 1986.

Fitzpatrick, J. J., Voigt, D. E., Fegyveresi, J. M., Stevens, N. T., Spencer, M. K., Cole-Dai, J., Alley, R. B., Jardine, G. E., Cravens, E. D., Wilen, L. A., Fudge, T., and Mcconnell, J. R.: Physical properties of the WAIS Divide ice core, Journal of Glaciology, 60, 1181–1198, https://doi.org/10.3189/2014JoG14J100, 2014.

Frank, F. C. and Read, W. T.: Multiplication Processes for Slow Moving Dislocations, Physical Review, 79, 722–723, https://doi.org/10.1103/PhysRev.79.722, https://link.aps.org/doi/10.1103/PhysRev.79.722, 1950.

Fujita, S., Hirabayashi, M., Goto-Azuma, K., Dallmayr, R., Satow, K., Zheng, J., and Dahl-Jensen, D.: Densification of layered firn of the ice sheet at NEEM, Greenland, Journal of Glaciology, 60, 905–921, https://doi.org/10.3189/2014JoG14J006, 2014.

Fukazawa, H., Sugiyama, K., Shinji, M., Narita, H., and Hondoh, T.: Acid ions at triple junction of Antarctic ice observed by Raman scattering, Geophysical Research Letters, 25, 2845–2848, 1998.

Glen, J. W.: The Effect of Hydrogen Disorder on Dislocation Movement and Plastic Deformation of Ice, Physik der kondensierten Materie, 7, 43–51, 1968.

645 Glen, J. W. and Jones, S. J.: The Deformation of Ice Single Crystals at Low Temperatures, Physics of Snow and Ice: proceedings, 1, 267–275, 1967.

Goldsby, D. L. and Kohlstedt, D. L.: Grain Boundary Sliding in Fine-grained Ice I, Scripta Materialia, 37, 1399–1406, 1997.

Gow, A. J. and Williamson, T.: Volcanic ash in the Antarctic Ice Sheet and its possible climatic implications, Earth and Planetary Science Letters, 13, 210–218, 1971.

650 Hobbs, P. V.: Ice physics, Oxford: Clarendon Press, Oxford, 1 edn., 1974.

Hörhold, M. W., Laepple, T., Freitag, J., Bigler, M., Fischer, H., and Kipfstuhl, S.: On the impact of impurities on the densification of polar firn, Earth and Planetary Science Letters, 325-326, 93–99, https://doi.org/10.1016/j.epsl.2011.12.022, 2012.

Hudson Institute of Mineralogy: mindat.org, https://www.mindat.org/acessed:05.05.2021, 2021.

Humphreys, F. and Hatherly, M.: Recrystallization and Related Annealing Phenomena, Elsevier, https://doi.org/10.1016/B978-0-08-044164-655 1.X5000-2, 2004.

Hvidberg, C. S., Grinsted, A., Dahl-Jensen, D., Khan, S. A., Kusk, A., Andersen, J. K., Neckel, N., Solgaard, A., Karlsson, N. B., Kjær, H. A., and Vallelonga, P.: Surface velocity of the Northeast Greenland Ice Stream (NEGIS): assessment of interior velocities derived from satellite data by GPS, The Cryosphere, 14, 3487–3502, https://doi.org/10.5194/tc-14-3487-2020, 2020.

Iliescu, D. and Baker, I.: Effects of impurities and their redistribution during recrystallization of ice crystals, Journal of Glaciology, 54, 660 362–370, 2008.

Jacka, T. and Li, J.: The steady-state crystal size of deforming ice, Annals of Glaciology, 20, 13–18, https://doi.org/10.1017/S0260305500016165, 1994.

Jones, S. J. and Glen, J. W.: The effect of dissolved impurities on the mechanical properties of ice crystals, Philosophical Magazine, 19, 13–24, https://doi.org/10.1080/14786436908217758, 1969.

665 Joughin, I., Smith, B. E., Howat, I. M., Scambos, T., and Moon, T.: Greenland flow variability from ice-sheet-wide velocity mapping, Journal of Glaciology, 56, 415–430, https://doi.org/10.3189/002214310792447734, 2010.

Joughin, I., Smith, B. E., and Howat, I. M.: A complete map of Greenland ice velocity derived from satellite data collected over 20 years, Journal of Glaciology, 64, 1–11, https://doi.org/10.1017/jog.2017.73, 2017.

Karato, S.-i., Toriumi, M., and Fujii, T.: Dynamic recrystallization of olivine single crystals during high-temperature creep, Geophysical 670 Research Letters, 7, 649–652, https://doi.org/10.1029/GL007i009p00649, 1980.

Kaufmann, P. R., Federer, U., Hutterli, M. A., Bigler, M., Schüpbach, S., Ruth, U., Schmitt, J., and Stocker, T. F.: An Improved Continuous Flow Analysis System for High-Resolution Field Measurements on Ice Cores, Environmental Science & Technology, 42, 8044–8050, https://doi.org/10.1021/es8007722, 2008.

Kipfstuhl, Sepp, Hamann, Ilka, Lambrecht, Anja, Freitag, Johannes, Faria, Sergio, H., Grigoriev, Dimitri, Azuma, and Nobuhiko: Microstruc-675 ture mapping: a new method for imaging deformation-induced microstructural features of ice on the grain scale, Journal of Glaciology, 52, 398–406, 2006.

Kuiper, E.-J. N., de Bresser, J. H. P., Drury, M. R., Eichler, J., Pennock, G. M., and Weikusat, I.: Using a composite flow law to model deformation in the NEEM deep ice core, Greenland – Part 2: The role of grain size and premelting on ice deformation at high homologous temperature, The Cryosphere, 14, 2449–2467, https://doi.org/10.5194/tc-14-2449-2020, 2020a.

680 Kuiper, E.-J. N., Weikusat, I., de Bresser, J. H. P., Jansen, D., Pennock, G. M., and Drury, M. R.: Using a composite flow law to model deformation in the NEEM deep ice core, Greenland – Part 1: The role of grain size and grain size distribution on deformation of the upper 2207 m, The Cryosphere, 14, 2429–2448, https://doi.org/10.5194/tc-14-2429-2020, 2020b.

Legrand, M. and Mayewski, P.: Glaciochemistry of polar ice cores: A review, Reviews of Geophysics, 35, 219–243, https://doi.org/10.1029/96RG03527, 1997.

685 Li, J., Jacka, T. H., and Morgan, V.: Crystal-size and microparticle record in the ice core from Dome Summit South, Law Dome, East Antarctica, Annals of Glaciology, 27, 343–348, 1998.

Lorius, C. J., Jouzel, C., Ritz, C., Merlivat, L., Barkov, N. I., Korotkevitch, Y. S., and Kotlyakov, V. M.: A 150 000 years climatic record from Antarctica, Nature, 316, 591–596, 1985.

Mader, H. M.: The thermal behaviour of the water-vein system in polyrystalline ice, Journal of Glaciology, 38, 359–374, 1992.

690 Masson-Delmotte, V., Stenni, B., Pol, K., Braconnot, P., Cattani, O., Falourd, S., Kageyama, M., Jouzel, J., Landais, A., Minster, B., Barnola, J. M., Chappellaz, J., Krinner, G., Johnsen, S., Röthlisberger, R., Hansen, J., Mikolajewicz, U., and Otto-Bliesner, B.: EPICA Dome C record of glacial and interglacial intensities, Quaternary Science Reviews, 29, 113–128, https://doi.org/10.1016/j.quascirev.2009.09.030, 2010.

McConnell, J. R., Lamorey, G. W., Lambert, S. W., and Taylor, K. C.: Continuous Ice-Core Chemical Analyses Using Inductively Coupled 695 Plasma Mass Spectrometry, Environmental Science & Technology, 36, 7–11, https://doi.org/10.1021/es011088z, 2002.

Minchew, B. M., Meyer, C. R., Robel, A. A., Gudmundsson, G. H., and Simons, M.: Processes controlling the downstream evolution of ice rheology in glacier shear margins: case study on Rutford Ice Stream, West Antarctica, Journal of Glaciology, 64, 583–594, https://doi.org/10.1017/jog.2018.47, 2018.

Minchew, B. M., Meyer, C. R., Pegler, S. S., Lipovsky, B. P., Rempel, A. W., Gudmundsson, G. H., and Iverson, N. R.: Comment on "Friction 700 at the bed does not control fast glacier flow", Science, 363, eaau6055, https://doi.org/10.1126/science.aau6055, 2019.

Mojtabavi, S., Wilhelms, F., Cook, E., Davies, S. M., Sinnl, G., Skov Jensen, M., Dahl-Jensen, D., Svensson, A., Vinther, B. M., Kipfstuhl, S., Jones, G., Karlsson, N. B., Faria, S. H., Gkinis, V., Kjær, H. A., Erhardt, T., Berben, S. M. P., Nisancioglu, K. H., Koldtoft, I., and Rasmussen, S. O.: A first chronology for the East Greenland Ice-core Project (EGRIP) over the Holocene and last glacial termination, Climate of the Past, 16, 2359–2380, https://doi.org/10.5194/cp-16-2359-2020, 2020.

705 Montagnat, M., Azuma, N., Dahl-Jensen, D., Eichler, J., Fujita, S., Gillet-Chaulet, F., Kipfstuhl, S., Samyn, D., Svensson, A., and Weikusat, I.: Fabric along the NEEM ice core, Greenland, and its comparison with GRIP and NGRIP ice cores, Cryosphere, 8, 1129–1138, https://doi.org/10.5194/tc-8-1129-2014, 2014.

Montagnat, M., Löwe, H., Calonne, N., Schneebeli, M., Matzl, M., and Jaggi, M.: On the Birth of Structural and Crystallographic Fabric Signals in Polar Snow: A Case Study From the EastGRIP Snowpack, Frontiers in Earth Science, 8, 1–23, 710 https://doi.org/10.3389/feart.2020.00365, 2020.

Moser, D. E., Hörhold, M., Kipfstuhl, S., and Freitag, J.: Microstructure of Snow and Its Link to Trace Elements and Isotopic Composition at Kohnen Station, Dronning Maud Land, Antarctica, Frontiers in Earth Science, 8, https://doi.org/10.3389/feart.2020.00023, 2020.

Nedelcu, A. F., Faria, S. H., and Kuhs, W. F.: Raman spectra of plate-like inclusions in the EPICA-DML (Antarctica) ice core, Journal of Glaciology, 55, 183–184, https://doi.org/10.3189/002214309788609010, 2009.

715 Ng, F. S. L.: Pervasive diffusion of climate signals recorded in ice-vein ionic impurities, The Cryosphere, 15, 1787–1810, https://doi.org/10.5194/tc-15-1787-2021, 2021.

Obbard, R. and Baker, I.: The microstructure of meteoric ice from Vostok , Antarctica, Journal of Glaciology, 53, 41–62, 2007.

Ohno, H., Igarashi, M., and Hondoh, T.: Salt inclusions in polar ice core: Location and chemical form of water-soluble impurities, Earth and Planetary Science Letters, 232, 171–178, https://doi.org/10.1016/j.epsl.2005.01.001, 2005.

720 Ohno, H., Igarashi, M., and Hondoh, T.: Characteristics of salt inclusions in polar ice from Dome Fuji, East Antarctica, Geophysical Research Letters, 33, L08 501, https://doi.org/10.1029/2006GL025774, 2006.

Ohno, H., Lipenkov, V. Y., and Hondoh, T.: Formation of air clathrate hydrates in polar ice sheets: heterogeneous nucleation induced by micro-inclusions, Journal of Glaciology, 56, 917–921, https://doi.org/10.3189/002214310794457317, 2010.

Ohno, H., Iizuka, Y., Horikawa, S., Sakurai, T., Hondoh, T., and Motoyama, H.: Potassium alum and aluminum sulfate micro-inclusions in
725 polar ice from Dome Fuji, East Antarctica, Polar Science, 8, 1–9, https://doi.org/10.1016/j.polar.2013.11.003, 2014.

Passchier, C. W. and Trouw, R. A. J.: Microtectonics, Springer-Verlag, Berlin/Heidelberg, 2 edn., https://doi.org/10.1007/3-540-29359-0, http://link.springer.com/10.1007/3-540-29359-0, 2005.

Paterson, W. S. B.: Why ice-age ice is sometimes "soft", Cold Regions Science and Technology, 20, 75–98, 1991.

Petit, J. R., Duval, P., and Lorius, C.: Long-term climatic changes indicated by crystal growth in polar ice, Nature, 326, 62–64, 1987.

730 Petit, J. R., Jouzel, J., Raynaud, D., Barkov, N. I., Barnola, J.-M., Basile, I., Bender, M., Chappellaz, J., Davisk, M., Delaygue, G., Delmotte, M., Kotlyakov, V. M., Legrand, M., Lipenkov, V. Y., Lorius, C., Pépin, L., Ritz, C., Saltzmank, E., and Stievenard, M.: Climate and atmospheric history of the past 420,000 years from the Vostok ice core, Antarctica The recent completion of drilling at Vostok station in East, Nature, 399, 429–436, 1999.

Petrenko, V. F. and Whitworth, R. W.: Physics of ice, Clarendon Press, London, 1999.

735 Piazolo, S., Montagnat, M., and Blackford, J. R.: Sub-structure characterization of experimentally and naturally deformed ice using cryo-EBSD, Journal of Microscopy, 230, 509–519, https://doi.org/10.1111/j.1365-2818.2008.02014.x, 2008.

Poirier, J.-P.: Creep of Crystals, Cambridge University Press, https://doi.org/10.1017/CBO9780511564451, 1985.

Rasmussen, S. O., Abbott, P. M., Blunier, T., Bourne, A. J., Brook, E., Buchardt, S. L., Buizert, C., Chappellaz, J., Clausen, H. B., Cook, E., Dahl-Jensen, D., Davies, S. M., Guillevic, M., Kipfstuhl, S., Laepple, T., Seierstad, I. K., Severinghaus, J. P., Steffensen, J. P., Stowasser,
740 C., Svensson, A., Vallelonga, P., Vinther, B. M., Wilhelms, F., and Winstrup, M.: A first chronology for the North Greenland Eemian Ice Drilling (NEEM) ice core, Climate of the Past, 9, 2713–2730, https://doi.org/10.5194/cp-9-2713-2013, https://cp.copernicus.org/articles/9/2713/2013/, 2013.

Reinhardt, H., Kriews, M., Miller, H., Schrems, O., Lüdke, C., Hoffmann, E., and Skole, J.: Laser ablation inductively coupled plasma mass spectrometry: a new tool for trace element analysis in ice cores, Fresenius' Journal of Analytical Chemistry, 370, 629–636,
745 https://doi.org/10.1007/s002160100853, 2001.

Röthlisberger, R., Bigler, M., Hutterli, M., Sommer, S., Stauffer, B., Junghans, H. G., and Wagenbach, D.: Technique for continuous high-resolution analysis of trace substances in firn and ice cores, Environmental Science and Technology, 34, 338–342, https://doi.org/10.1021/es9907055, 2000.

Ruth, U., Wagenbach, D., Steffensen, J. P., and Bigler, M.: Continuous record of microparticle concentration and size distribution
750 in the central Greenland NGRIP ice core during the last glacial period, Journal of Geophysical Research: Atmospheres, 108, https://doi.org/10.1029/2002JD002376, 2003.

Rutter, E. H.: Experimental study of the influence of stress, temperature, and strain on the dynamic recrystallization of Carrara marble, Journal of Geophysical Research: Solid Earth, 100, 24 651–24 663, https://doi.org/10.1029/95JB02500, 1995.

Sakurai, T., Ilzuka, Y., Horlkawa, S., Johnsen, S., Dahl-Jensen, D., Steffensen, J. P., and Hondoh, T.: Direct observation of salts as micro-inclusions in the Greenland GRIP ice core, Journal of Glaciology, 55, 777–783, https://doi.org/10.3189/002214309790152483, 2009.

Sakurai, T., Ohno, H., Genceli, F. E., Horikawa, S., Iizuka, Y., Uchida, T., and Hondoh, T.: Magnesium methanesulfonate salt found in the Dome Fuji (Antarctica) ice core, Journal of Glaciology, 56, 837–842, https://doi.org/10.3189/002214310794457335, 2010.

Sakurai, T., Ohno, H., Horikawa, S., Iizuka, Y., Uchida, T., Hirakawa, K., and Hondoh, T.: The chemical forms of water-soluble microparticles preserved in the Antarctic ice sheet during Termination I, Journal of Glaciology, 57, 1027–1032, https://doi.org/10.3189/002214311798843403, 2011.

Severi, M., Becagli, S., Frosini, D., Marconi, M., Traversi, R., and Udisti, R.: A Novel Fast Ion Chromatographic Method for the Analysis of Fluoride in Antarctic Snow and Ice, Environmental Science & Technology, 48, 1795–1802, https://doi.org/10.1021/es404126z, 2014.

Shigeyama, W., Nagatsuka, N., Homma, T., Takata, M., Goto-Azuma, K., Weikusat, I., Drury, M. R., Kuiper, E. J. N., Mateiu, R. V., Azuma, N., Dahl-Jensen, D., and Kipfstuhl, S.: Microstructural analysis of Greenland ice using a cryogenic scanning electron microscope equipped with an electron backscatter diffraction detector, Bulletin of Glaciological Research, 37, 31–45, https://doi.org/10.5331/BGR.19R01, 2019.

Simonsen, M. F., Baccolo, G., Blunier, T., Borunda, A., Delmonte, B., Frei, R., Goldstein, S., Grinsted, A., Kjær, H. A., Sowers, T., Svensson, A., Vinther, B., Vladimirova, D., Winckler, G., Winstrup, M., and Vallelonga, P.: East Greenland ice core dust record reveals timing of Greenland ice sheet advance and retreat, Nature Communications, 10, https://doi.org/10.1038/s41467-019-12546-2, http://dx.doi.org/10.1038/s41467-019-12546-2, 2019.

Smith, C. S.: Grains, phases, and interfaces: An introduction of microstructure, Trans. AIME, 175, 15–51, 1948.

Spaulding, N. E., Sneed, S. B., Handley, M. J., Bohleber, P., Kurbatov, A. V., Pearce, N. J., Erhardt, T., and Mayewski, P. A.: A New Multielement Method for LA-ICP-MS Data Acquisition from Glacier Ice Cores, Environmental Science & Technology, 51, 13 282–13 287, https://doi.org/10.1021/acs.est.7b03950, 2017.

Stearns, L. A. and van der Veen, C.: Response to Comment on "Friction at the bed does not control fast glacier flow", Science, 363, eaau8375, https://doi.org/10.1126/science.aau8375, https://www.sciencemag.org/lookup/doi/10.1126/science.aau8375, 2019.

Steffensen, J. P.: The size distribution of microparticles from selected segments of the Greenland Ice Core Project ice core representing different climatic periods, Journal of Geophysical Research, 102, 755–2, 1997.

Steinbach, F., Kuiper, E.-J. N., Eichler, J., Bons, P. D., Drury, M. R., Griera, A., Pennock, G. M., and Weikusat, I.: The Relevance of Grain Dissection for Grain Size Reduction in Polar Ice: Insights from Numerical Models and Ice Core Microstructure Analysis, Frontiers in Earth Science, 5, https://doi.org/10.3389/feart.2017.00066, 2017.

Stillman, D. E., MacGregor, J. A., and Grimm, R. E.: The role of acids in electrical conduction through ice, Journal of Geophysical Research: Earth Surface, 118, 1–16, https://doi.org/10.1029/2012JF002603, http://doi.wiley.com/10.1029/2012JF002603, 2013.

Stipp, M. and Tullis, J.: The recrystallized grain size piezometer for quartz, Geophysical Research Letters, 30, 2088, https://doi.org/10.1029/2003GL018444, 2003.

Stoll, N., Eichler, J., Hörhold, M., Erhardt, T., Jensen, C., and Weikusat, I.: Microstructure, Micro-inclusions and Mineralogy along the EGRIP ice core - Part 2: Implications for paleo-mineralogy, The Cryosphere Discussions, pp. 1–30, https://doi.org/https://doi.org/10.5194/tc-2021-190, 2021a.

Stoll, N., Eichler, J., Hörhold, M., Shigeyama, W., and Weikusat, I.: A Review of the Microstructural Location of Impurities and Their Impacts on Deformation, Frontiers in Earth Science, 8, https://doi.org/10.3389/feart.2020.615613, 2021b.

790 Svensson, A., Nielsen, S. W., Kipfstuhl, S., Johnsen, S. J., Steffensen, J. P., Bigler, M., Ruth, U., and Röthlisberger, R.: Visual stratigraphy of the North Greenland Ice Core Project (NorthGRIP) ice core during the last glacial period, Journal of Geophysical Research, 110, 1–11, https://doi.org/10.1029/2004JD005134, 2005.

Thorsteinsson, T., Kipfstuhl, J., and Miller, H.: Textures and fabrics in the GRIP ice core, Journal of Geophysical Research: Oceans, 102, 26 583–26 599, https://doi.org/10.1029/97JC00161, 1997.

795 Treverrow, A., Budd, W. F., Jacka, T. H., and Warner, R. C.: The tertiary creep of polycrystalline ice: experimental evidence for stress-dependent levels of strain-rate enhancement, Journal of Glaciology, 58, 301–314, https://doi.org/10.3189/2012JoG11J149, 2012.

Vallelonga, P., Christianson, K., Alley, R. B., Anandakrishnan, S., Christian, J. E., Dahl-Jensen, D., Gkinis, V., Holme, C., Jacobel, R. W., Karlsson, N. B., Keisling, B. A., Kipfstuhl, S., Kjær, H. A., Kristensen, M. E., Muto, A., Peters, L. E., Popp, T., Riverman, K. L., Svensson, A. M., Tibuleac, C., Vinther, B. M., Weng, Y., and Winstrup, M.: Initial results from geophysical surveys and shallow coring of 800 the Northeast Greenland Ice Stream (NEGIS), Cryosphere, 8, 1275–1287, https://doi.org/10.5194/tc-8-1275-2014, 2014.

Walker, M., Head, M. J., Berkelhammer, M., Björck, S., Cheng, H., Cwynar, L., Fisher, D., Gkinis, V., Long, A., Lowe, J., Newnham, R., Rasmussen, S. O., and Weiss, H.: Formal ratification of the subdivision of the Holocene Series/Epoch (Quaternary System/Period): two new Global Boundary Stratotype Sections and Points (GSSPs) and three new stages/subseries, Episodes, 41, 213–223, https://doi.org/10.18814/epiiugs/2018/018016, 2018.

805 Wang, Y., Thorsteinsson, T., Kipfstuhl, J., Miller, H., Dahl-Jensen, D., and Shoji, H.: A vertical girdle fabric in the NorthGRIP deep ice core, North Greenland, Annals of Glaciology, 35, 515–520, https://doi.org/10.3189/172756402781817301, 2002.

Watanabe, O., Jouzel, J., Johnsen, S., Parrenin, F., Shoji, H., and Yoshida, N.: Homogeneous climate variability across East Antarctica over the past three glacial cycles, Nature, 422, 509–512, https://doi.org/10.1038/nature01525, 2003.

Weertman, J.: Creep of Ice, in: Physics and Chemistry of Ice, edited by Whalley, E., Jones, S. W., and Gold, L. W., pp. 320–37, Royal Society 810 of Canada, Ottawa, 1973.

Weertman, J. and Weertman, J. R.: Elementary Dislocation Theory, Oxford University Press, Oxford, 1992.

Wegner, A., Fischer, H., Delmonte, B., Petit, J.-R., Erhardt, T., Ruth, U., Svensson, A., Vinther, B., and Miller, H.: The role of seasonality of mineral dust concentration and size on glacial/interglacial dust changes in the EPICA Dronning Maud Land ice core, Journal of Geophysical Research: Atmospheres, 120, 9916–9931, https://doi.org/10.1002/2015JD023608, 2015.

815 Weikusat, C., Freitag, J., and Kipfstuhl, S.: Raman spectroscopy of gaseous inclusions in EDML ice core: first results – microbubbles, Journal of Glaciology, 58, 761–766, https://doi.org/10.3189/2012JoG11J222, 2012.

Weikusat, I., Kipfstuhl, S., Faria, S. H., Azuma, N., and Miyamoto, A.: Subgrain boundaries and related microstructural features in EDML (Antarctica) deep ice core, Journal of Glaciology, 55, 461–472, https://doi.org/10.3189/002214309788816614, 2009.

Weikusat, I., Miyamoto, A., Faria, S. H., Kipfstuhl, S., Azuma, N., and Hondoh, T.: Subgrain boundaries in Antarctic ice quantified by X-ray 820 Laue diffraction, Journal of Glaciology, 57, 111–120, https://doi.org/10.3189/002214311795306628, 2011.

Weikusat, I., Jansen, D., Binder, T., Eichler, J., Faria, S. H., Wilhelms, F., Kipfstuhl, S., Sheldon, S., Miller, H., Dahl-Jensen, D., and Kleiner, T.: Physical analysis of an Antarctic ice core—towards an integration of micro- and macrodynamics of polar ice, Philosophical Transactions of the Royal Society A: Mathematical, Physical and Engineering Sciences, 375, 20150 347, https://doi.org/10.1098/rsta.2015.0347, 2017a.

825 Weikusat, I., Kuiper, E. J. N., Pennock, G. M., Kipfstuhl, S., and Drury, M. R.: EBSD analysis of subgrain boundaries and dislocation slip systems in Antarctic and Greenland ice, Solid Earth, 8, 883–898, https://doi.org/10.1159/000320310, 2017b.

Weikusat, I., Westhoff, J., Kipfstuhl, S., and Jansen, D.: Visual stratigraphy of the EastGRIP ice core (14 m - 2021 m depth, drilling period 2017-2019), https://doi.org/10.1594/PANGAEA.925014, https://doi.org/10.1594/PANGAEA.925014, 2020.

Weiss, J., Vidot, J., Gay, M., Arnaud, L., Duval, P., and Petit, J. R.: Dome Concordia ice microstructure: impurities effect on grain growth, Annals of Glaciology, 35, 552–558, https://doi.org/10.3189/172756402781816573, 2002.

Westhoff, J., Stoll, N., Franke, S., Weikusat, I., Bons, P., Kerch, J., Jansen, D., Kipfstuhl, S., and Dahl-Jensen, D.: A stratigraphy-based method for reconstructing ice core orientation, Annals of Glaciology, pp. 1–12, https://doi.org/10.1017/aog.2020.76, 2020.

Wilhelms, F., Kipfstuhl, J., Miller, H., Heinloth, K., and Firestone, J.: Precise dielectric profiling of ice cores: a new device with improved guarding and its theory, Journal of Glaciology, 44, 171–174, 1998.

Wilson, C. J., Russell-Head, D. S., and Sim, H. M.: The application of an automated fabric analyzer system to the textural evolution of folded ice layers in shear zones, Annals of Glaciology, 37, 7–17, https://doi.org/10.3189/172756403781815401, 2003.

Wolff, E. W., Miners, W. D., Moore, J. C., and Paren, J. G.: Factors Controlling the Electrical Conductivity of Ice from the Polar Regions-A Summary, The Journal of Physical Chemistry B, 101, 6090–6094, https://doi.org/10.1021/jp9631543, 1997.

Yakobi-Hancock, J. D., Ladino, L. A., and Abbatt, J. P. D.: Feldspar minerals as efficient deposition ice nuclei, Atmospheric Chemistry and Physics, 13, 11 175–11 185, https://doi.org/10.5194/acp-13-11175-2013, 2013.